

Review

Advancements in Lithium–Oxygen Batteries: A Comprehensive Review of Cathode and Anode Materials

Jing Guo ^{1,2,3}, Xue Meng ^{1,2,3}, Qing Wang ^{1,2,3}, Yahui Zhang ^{1,2,3}, Shengxue Yan ^{1,2,3} and Shaohua Luo ^{1,2,3,*}

¹ School of Materials Science and Engineering, Northeastern University, Shenyang 110819, China; guojing@neuq.edu.cn (J.G.)

² School of Resources and Materials, Northeastern University at Qinhuangdao, Qinhuangdao 066004, China

³ Hebei Key Laboratory of Dielectric and Electrolyte Functional Material, Qinhuangdao 066004, China

* Correspondence: luosh@neuq.edu.cn

Abstract: As modern society continues to advance, the depletion of non-renewable energy sources (such as natural gas and petroleum) exacerbates environmental and energy issues. The development of green, environmentally friendly energy storage and conversion systems is imperative. The energy density of commercial lithium-ion batteries is approaching its theoretical limit, and even so, it struggles to meet the rapidly growing market demand. Lithium–oxygen batteries have garnered significant attention from researchers due to their exceptionally high theoretical energy density. However, challenges such as poor electrolyte stability, short cycle life, low discharge capacity, and high overpotential arise from the sluggish kinetics of the oxygen reduction reaction (ORR) during discharge and the oxygen evolution reaction (OER) during charging. This article elucidates the fundamental principles of lithium–oxygen batteries, analyzes the primary issues currently faced, and summarizes recent research advancements in air cathodes and anodes. Additionally, it proposes future directions and efforts for the development of lithium–air batteries.

Keywords: lithium–oxygen battery; electrode material; catalyst; first principles; electrochemical performance



Citation: Guo, J.; Meng, X.; Wang, Q.; Zhang, Y.; Yan, S.; Luo, S.

Advancements in Lithium–Oxygen Batteries: A Comprehensive Review of Cathode and Anode Materials. *Batteries* **2024**, *10*, 260. <https://doi.org/10.3390/batteries10080260>

Academic Editor: Hirotoshi Yamada

Received: 4 June 2024

Revised: 5 July 2024

Accepted: 16 July 2024

Published: 23 July 2024



Copyright: © 2024 by the authors. Licensee MDPI, Basel, Switzerland. This article is an open access article distributed under the terms and conditions of the Creative Commons Attribution (CC BY) license (<https://creativecommons.org/licenses/by/4.0/>).

1. Introduction

The extensive utilization of fossil fuels has played a significant role in promoting economic success and enhancing living conditions. However, it has also intensified the problems of global warming and environmental pollution. The worldwide community has shown significant interest in the long-term viability of energy provision. It is crucial to decrease the use of fossil fuels and promote the advancement of environmentally friendly, renewable, and non-polluting energy sources, including solar, wind, hydro, and tidal power [1–3]. However, these technologies are susceptible to natural environmental conditions and geographical locations, leading to inherent uncontrollability and intermittent supply issues. Hence, the imperative lies in the advancement of energy storage systems that are both eco-friendly, technologically advanced, and cost-effective. Presently, there exists a multitude of rechargeable batteries, including lithium-ion batteries [4], which have advanced significantly and are now widely utilized because of their inexpensive, high energy density, and favorable environmental compatibility [5–7]. However, the energy density of traditional lithium-ion batteries has approached its theoretical limit, necessitating the development of battery systems with higher energy density [8–10].

Metal–air batteries, as representatives of the new generation of green secondary batteries, have an exceptionally high theoretical energy density and are expected to play a significant role in electric transportation and energy storage [11]. Rechargeable lithium–oxygen ($\text{Li}-\text{O}_2$) batteries boast a satisfactory theoretical energy density ($11,400 \text{ Wh kg}^{-1}$, based on pure lithium), nearly equivalent to gasoline ($12,800 \text{ Wh kg}^{-1}$); the actual energy density also approaches that of gasoline, at approximately 1700 Wh kg^{-1} . Even based

on Li_2O_2 calculations, $\text{Li}-\text{O}_2$ batteries exhibit a high specific energy density of up to 3500 Wh kg^{-1} . Given its abundance and low cost, oxygen may be readily acquired from the air and used as the electrode reactant, showing great potential in the fields of energy storage and conversion [12,13]. Through continuous efforts by researchers, significant progress has been made in the charging and discharging mechanisms, electrode/electrolyte design, and performance optimization of $\text{Li}-\text{O}_2$ batteries, demonstrating vast development prospects [14].

However, the development of this system is still in its early stages, with numerous key scientific issues and technological bottlenecks yet to be resolved. The actual performance of the battery, such as energy conversion efficiency, rate capability, and cycling performance, has far from reached the standards for commercial applications. Additionally, some technological bottlenecks, such as the development and preparation of inexpensive bifunctional catalysts and the corrosion prevention of active metal negative electrodes, result in difficulties in decomposing discharge products, electrolyte decomposition, short cycle life, dendrite growth, parasitic reactions, and slow reaction kinetics, becoming obstacles in the commercialization process of $\text{Li}-\text{O}_2$ batteries. Hence, the advancement of exceptionally efficient and enduring electrode materials is of utmost importance to facilitate the widespread implementation of $\text{Li}-\text{O}_2$ batteries in industries.

2. Basic Principles and Fundamental Issues of Lithium–Oxygen Batteries

Among all rechargeable metal–air batteries, $\text{Li}-\text{O}_2$ batteries (typically aprotic $\text{Li}-\text{O}_2$ batteries) have the highest theoretical energy density. Based solely on the mass of the lithium metal anode, the theoretical energy density of $\text{Li}-\text{O}_2$ batteries can reach $11,400 \text{ Wh kg}^{-1}$. When considering the masses of both Li and Li_2O_2 , the theoretical energy density of $\text{Li}-\text{O}_2$ batteries remains impressively high at 3505 Wh kg^{-1} , which is significantly higher than that of lithium-ion batteries (LIBs) [15]. The remarkable energy density of $\text{Li}-\text{O}_2$ batteries is mainly due to two factors: first, the cathode material, oxygen, is obtained from the surrounding environment instead of being kept within the battery, resulting in a decrease in the weight of the completed battery. Furthermore, as the battery is being discharged, the lithium anode exhibits a remarkably high specific capacity and a comparatively low electrochemical potential (versus the standard hydrogen electrode (SHE) at -3.04 V), ensuring ideal discharge capacity and high operating voltage [16].

2.1. Basic Principles of Lithium–Oxygen Batteries

A typical non-aqueous $\text{Li}-\text{O}_2$ battery consists of a lithium metal anode, a non-aqueous electrolyte (comprising organic solvents and lithium salts), a separator, and a porous cathode. The porous cathode does not contribute directly to energy storage as an active material (Figure 1). Instead, it functions as a gas transport channel, an electron conduction medium, a host matrix for discharge products (non-catalytic role), and as a catalyst for the nucleation, growth, and decomposition of discharge products (catalytic role) [17]. During discharge, lithium metal loses electrons to form lithium ions (Li^+). The Li^+ ions react with oxygen and electrons from the external circuit to produce lithium peroxide, which is the discharge product (Li_2O_2), which deposits on the cathode material. The reaction process is as follows:



During the subsequent charging process, Li_2O_2 decomposes into oxygen and Li^+ , which then combine with electrons transferred from the external circuit to form metallic lithium. The reactions are as follows:



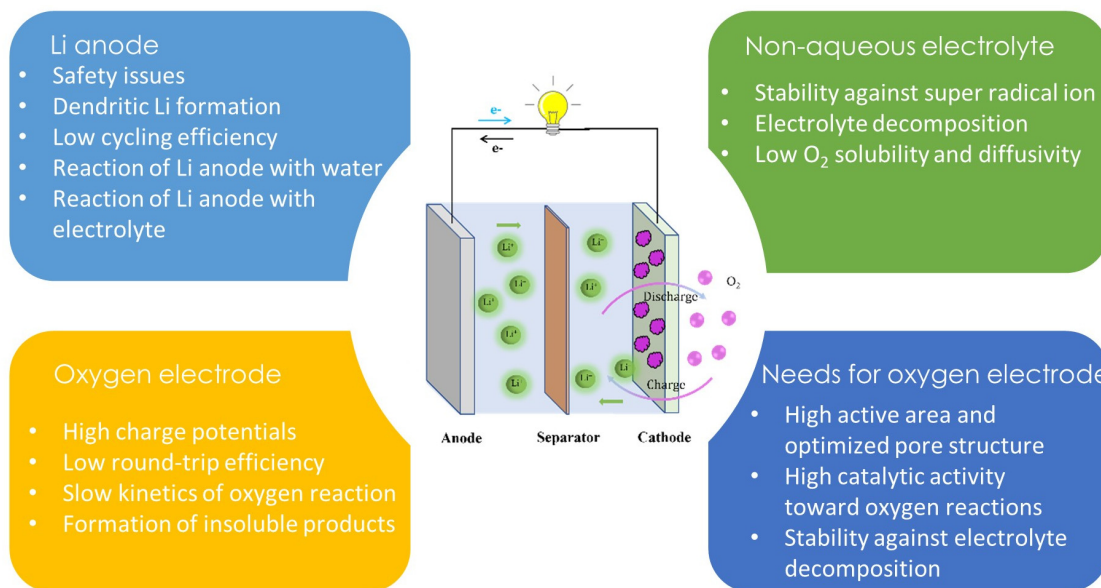


Figure 1. Components and technical challenges of rechargeable $\text{Li}-\text{O}_2$ battery.

2.2. Fundamental Issues in Lithium–Oxygen Batteries

The internal redox reactions in $\text{Li}-\text{O}_2$ batteries are notably complex due to the occurrence of oxygen reduction and oxygen evolution reactions at the gas–liquid–solid three-phase interface. Despite the significant advantages of lithium–oxygen batteries, research on this battery system is still in its infancy. The determinants impacting the charge and discharge mechanisms are inadequately comprehended, and extensive research is required to achieve commercial applications. The current challenges faced by $\text{Li}-\text{O}_2$ batteries include:

Reactive Lithium Metal Anode: The lithium anode readily reacts with atmospheric CO_2 and H_2O , leading to anode degradation. Additionally, the electrolyte tends to decompose during charge and discharge cycles, generating water, which further exacerbates the degradation of the lithium anode, significantly increasing safety risks. Moreover, the high reactivity of lithium metal can lead to the formation of dendrites, therefore shortening the battery's lifespan.

Accumulation of Discharge Products: During discharge, O_2 is sequentially converted to superoxide and lithium peroxide. As these reactions proceed, the discharge products continuously accumulate, which can corrode battery components and reduce the battery's endurance capacity.

Poor Cycling Stability: Lithium peroxide, the discharge product, has very low solubility in the electrolyte, causing it to accumulate on the electrode, which can terminate the discharge process and adversely affect the battery's cycle life. Additionally, high overpotentials can negatively impact the cycling stability of the battery.

High Overpotential: This significantly reduces the charge–discharge efficiency compared to lithium-ion batteries. The primary cause is the high overpotential required to decompose the discharge products. An effective approach to address this problem is to design highly efficient bifunctional catalysts capable of facilitating both the ORR and OER.

To advance the commercialization of $\text{Li}-\text{O}_2$ batteries, it is crucial to develop highly active and stable electrode materials that can overcome these challenges.

3. Advances in Anode Material Research

Organic-based metal–air batteries have become a research hotspot in recent years due to their high theoretical energy density. Taking $\text{Li}-\text{O}_2$ batteries as an example, the

typical structure of an organic-based Li–O₂ battery consists of a lithium anode, an organic electrolyte containing Li⁺, and a cathode material. Currently, most Li–O₂ battery research focuses on the cathode interface reactions. However, the highly reductive nature of the lithium anode leads to side reactions, complicating the reactions involved in Li–O₂ batteries. Oxygen and electrolytes diffusing from the cathode can react with the lithium anode; simultaneously, by-products generated at the lithium anode can diffuse to the cathode, interfering with cathode reactions. Additionally, the potential formation of dendrites on the anode significantly reduces the battery's safety, hindering the practical application of the Li–O₂ battery system. Therefore, it is urgent to study and resolve the stability and safety issues within the metal lithium anode. Below is a brief overview of the latest research on the protection and modification of lithium anodes in organic-based Li–O₂ batteries.

3.1. Strategies for Lithium Anode Alternatives (Non-Pure Lithium Anodes)

Given the similarities between Li–O₂ batteries and lithium metal batteries, insights can be drawn from the development of lithium metal batteries. Using anode materials from lithium-ion batteries instead of lithium metal can address the dendrite issue, making this a viable approach for Li–O₂ batteries. Lithium-ion batteries offer a notable benefit by utilizing lithium-intercalated graphite anodes in place of lithium metal. Intercalated carbon materials can create LiC₆, which has a theoretical specific capacity of 372 mAh g⁻¹. However, this capacity seems to be reduced when used in Li–O₂ batteries. To address this issue, Hirshberg et al. introduced the concept of lithiated hard carbon as an alternative anode material for Li–O₂ batteries. This material offers a higher specific capacity compared to lithiated graphite [18]. Fully charged batteries operated for nearly 30 cycles. While the process of introducing lithium ions into hard carbon is significantly safer, it is important to note that hard carbon is not a cost-effective option. In addition to carbon materials, Si, Sn, and Al can combine with Li to create alloys that can be used as anodes containing lithium. Silicon, which has great potential as an anode material in lithium-ion batteries, has also been thoroughly investigated for its use in lithium–oxygen batteries [19–22].

Zhou's research team has effectively created a high-performing lithium-ion oxygen (Li–O₂) battery by utilizing commercially available silicon (Si) particles as the anode [22]. A robust solid–electrolyte interface (SEI) coating was formed on the surface of the silicon (Si) anode. This enhanced solid–electrolyte interphase (SEI) film not only improves the long-term durability of the silicon (Si) electrode in cycling but also functions as a protective barrier to effectively inhibit the undesired chemical reactions induced by oxygen diffusion into the anode. The study reveals that the SEI film contains organic substances, lithium carbonate (Li₂CO₃), lithium fluoride (LiF), and specific fluorocarbon compounds. These components endow the Si electrode with protection against oxidative side reactions, thus achieving superior battery performance. The Li–O₂ battery demonstrated excellent cycling stability, capable of undergoing 100 discharge–charge cycles at low overpotentials. In addition, the energy density of this Li-ion O₂ battery has reached 678 Wh kg⁻¹, which is considerably higher than that of traditional lithium-ion batteries (384 Wh kg⁻¹), and it is anticipated to have a maximum energy density of 1764 Wh kg⁻¹ (Figure 2a–c). Experiments also confirmed the long-term cycling potential of these Li–O₂ batteries.

Researchers have also synthesized and directly utilized lithium-rich Li–Si alloys (e.g., Li₂₂Si₅ and Li₁₃Si₄) as anode materials for air batteries. X-ray diffraction (XRD) analysis revealed that the formation of charge products (Li_xSi_y phases) during discharge/charge cycles is directly influenced by the stoichiometry of the initial alloy anode. Under a fixed capacity condition (800 mAh g⁻¹), the assembled Li–O₂ battery exhibited a specific energy density of approximately 1840 Wh kg⁻¹, with an operating voltage of around 2.3 V. The use of Li–Si alloy anodes in Li–air batteries demonstrated high Coulombic efficiency (approximately 97%) and low polarization (around 1.7 V), indicating excellent electrochemical performance [23]. The Li–Si alloy anodes effectively mitigate the reactivity of metallic lithium anodes and address issues related to volume changes during the Si charge–discharge process. These alloys, which do not require electrochemical lithiation, are easy to

scale up for practical applications, showcasing significant potential as anode materials in Li–O₂ batteries. Among them, the Li₂₂Si₅ alloy, due to its high lithium content, exhibited particularly satisfactory electrochemical performance (Figure 2d). This advancement underscores the viability of using Li–Si alloys to enhance the stability, efficiency, and scalability of next-generation lithium–air batteries, highlighting their potential for achieving superior energy storage solutions.

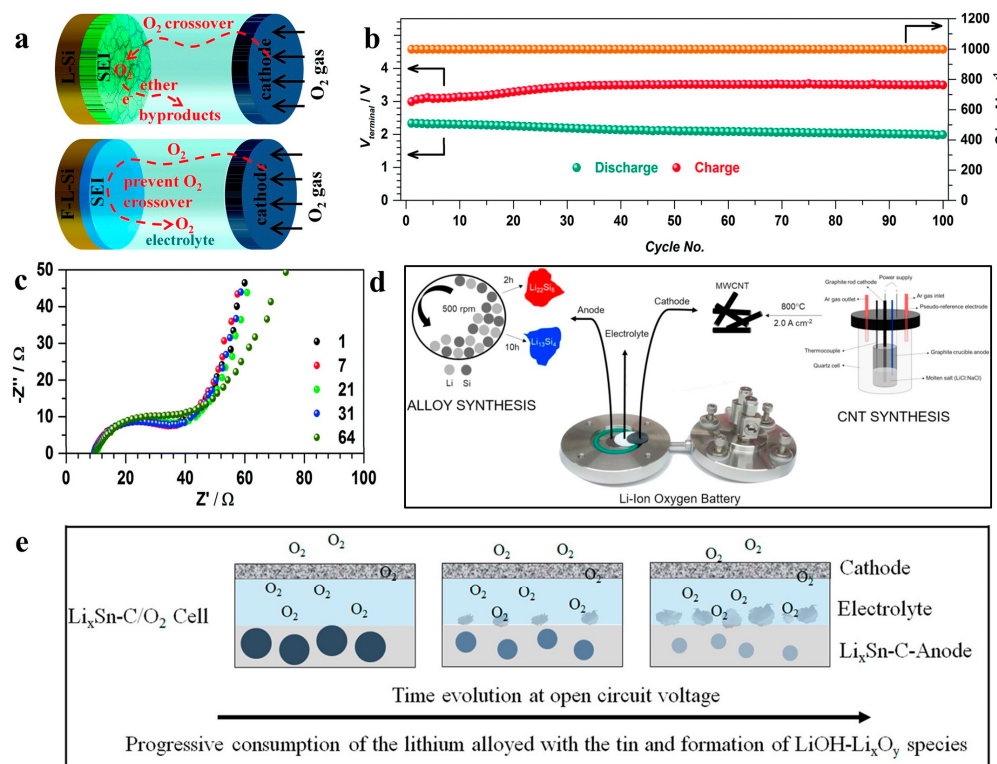


Figure 2. (a) SEI film evolution of L–Si and F–L–Si anodes in Li-ion O₂ batteries during the discharge–charge cycle and their resistibility towards the O₂ crossover effect on Si anodes. (b) The specific capacities along with discharge and charge terminal voltages against cycle number of Li-ion O₂ batteries with F–L–Si anodes. (c) The corresponding electrochemical impedance spectrum (EIS) of the discharged Li-ion O₂ batteries with F–L–Si anodes [22]. Copyright 2016, The Royal Society of Chemistry. (d) Schematics of the electrode preparation and Li-ion oxygen battery assembling [23]. Copyright 2021, Elsevier. (e) Schematic representation of the reactions occurring at the electrode/electrolyte interphase of a Li_xSn–C/Pyr₁₄TFSI–LiTFSI/O₂ cell in the OCV condition under an oxygen atmosphere [24]. Copyright 2015, American Chemical Society.

Under an Ar atmosphere, silicon and lithium powders are ball-milled into lithium–silicon alloy powder, directly used as the anode in Li–O₂ batteries. The extended lifespan of batteries containing commercial silicon can be linked to the formation of a robust solid–electrolyte interphase (SEI) film on the surface of the silicon anode (Figure 2e). This film acts as a barrier, preventing oxygen from crossing over and suppressing unwanted interactions between the anode and electrolyte. Elia et al. conducted a study on the use of Sn-based anodes in Li–O₂ batteries. They found that the inclusion of Sn nanoparticles in a carbon matrix of micron size improved the mechanical stability of the anodes [24]. Nevertheless, batteries equipped with these anodes had a limited lifespan of only nine cycles. The decrease in the discharge and charge voltage distributions was a result of the irreversible consumption of the anode. The ongoing production of LiOH and Li_xO_y on the surface of the Li_xSnC anode resulted in the permanent depletion of the available lithium source on the anode, ultimately leading to the failure of the battery. Additionally, lithiated Al–C composite electrodes were prepared electrochemically and applied to Li–O₂ batteries.

Compared to batteries with a metallic Li anode, those using Li_xAlC anodes exhibited better cycling performance [25].

Besides the aforementioned anodes, special cathode materials such as LiFePO_4 are often used as anodes in $\text{Li}-\text{O}_2$ batteries. This material acts as a reference electrode, stabilizing at approximately 3.45 V relative to Li/Li^+ , and involves a two-phase reaction between $\text{Li}_{1-x}\text{FePO}_4$ and FePO_4 . It exhibits higher resistance to oxidation caused by oxygen in the electrolyte and can minimize the presence of impurities resulting from the breakdown of the electrolyte at the lithium anode. Consequently, a cleaner electrochemical system for $\text{Li}-\text{O}_2$ batteries can be achieved [26,27]. However, due to the high potential of LiFePO_4 , it is impractical to use it as an anode material for $\text{Li}-\text{O}_2$ batteries.

3.2. Electrolyte Design

The electrically insulating and ionically conducting solid–electrolyte interphase (SEI) film is rapidly formed at the interface between the anode and the electrolyte. This film effectively protects the lithium metal from corrosion. This film is typically delicate and susceptible to fracturing while being transported on a bicycle.

Introducing N,N-Dimethyltrifluoroacetamide (DMTFA) into $\text{Li}-\text{O}_2$ batteries helps form a stable SEI film in the presence of N,N-Dimethylacetamide (DMA), preventing sustained reactions with lithium metal [28]. They also developed DMA-based $\text{Li}-\text{O}_2$ batteries using LiNO_3 as the electrolyte salt [29].

A stable solid–electrolyte interface (SEI) coating effectively inhibits the reactions between metallic lithium and the electrolyte [29]. LiNO_3 can serve as a co-additive with vinylene carbonate (VC) in $\text{Li}-\text{O}_2$ batteries [30]. In this investigation, the electrolyte consisted of LiClO_4 /dimethyl sulfoxide (DMSO). By adding VC and LiNO_3 , the Coulombic efficiency increased from 25% to 82.5%. Another inorganic salt, InI_3 , proposed by Zhou's group, serves as an effective additive for $\text{Li}-\text{O}_2$ batteries [31]. This additive combines the redox mediator (RM) and lithium protection in an inventive way. The discharge product Li_2O_2 is oxidized by soluble I_3^- ions, which function as the redox mediator [32]. However, when oxidant I_3^- interacts with metallic lithium in the system, it may shuttle to the negative electrode, as it takes several minutes to oxidize Li_2O_2 . Huang's group has proposed the use of boric acid (BA) as an additive for forming a solid–electrolyte interphase (SEI) on lithium metal surfaces [33]. This approach facilitates the formation of a continuous and dense SEI layer composed of nanocrystalline lithium borates and amorphous borates. The resulting SEI film exhibits excellent ionic conductivity and mechanical strength, effectively inhibiting the permeation of oxygen and electrolyte solvents as well as the growth of lithium dendrites. Thanks to the inclusion of BA, the cycle life of lithium–oxygen batteries (LOBs) has been extended by more than six times. Researchers believe this method offers a promising solution to enhance the stability of lithium metal anodes, making practical, rechargeable LOBs a viable reality. This innovation underscores the potential of boric acid as an effective strategy for improving the durability and performance of next-generation energy storage systems (Figure 3a,b).

$\text{Li}-\text{O}_2$ batteries have utilized solid-state electrolytes such as solid polymer and ceramic electrolytes. Currently, two types with high ionic conductivity (in the range of 10^{-4} – 10^{-3} S cm $^{-1}$), $\text{Li}-\text{Al}-\text{Ge}-\text{PO}_4$ (LAGP) [11] and $\text{Li}-\text{Al}-\text{Ti}-\text{PO}_4$ (LATP) [36], have been used in $\text{Li}-\text{O}_2$ batteries. However, the performance is not satisfactory. Therefore, Zhou et al. introduced a polymer/ceramic/polymer electrolyte [37]. In this structure, the binding between LATP and cross-linked poly(ethylene glycol) methyl ether acrylate provides an effective soft interface and high mechanical strength ceramic blocks. Using a polypropylene–poly(methyl methacrylate)–polystyrene nanocomposite with SiO_2 as the electrolyte for $\text{Li}-\text{O}_2$ batteries, this electrolyte exhibits lower interfacial resistance with the lithium anode compared to liquid electrolytes, showing better compatibility with the lithium metal anode and improving long-term cycling performance [38]. Jang et al. studied the effect of a poly(vinylidene fluoride–co-hexafluoropropylene) (PVdF-HFP) coating on the cycling stability of $\text{Li}-\text{O}_2$ batteries [39]. The PVdF-HFP coating reduces interface resistance during

charge and discharge and suppresses dendritic growth, therefore improving the cycling stability of Li–O₂ batteries. Subsequently, the Peng group also developed all-solid-state Li–O₂ batteries mainly composed of polymer electrolytes, primarily consisting of PVdF–HFP [34]. The researchers initially created an innovative Li–O₂ battery that consists of fibers. This battery exhibits excellent electrochemical performance and is also flexible. The battery's discharge capacity is 12,470 milliampere-hours per gram (mAh g⁻¹), and it can consistently function for 100 cycles in an ambient environment, maintaining good electrochemical performance after bending and twisting. It can also be wearable, forming flexible power textiles for various electronic devices (Figure 3c–e).

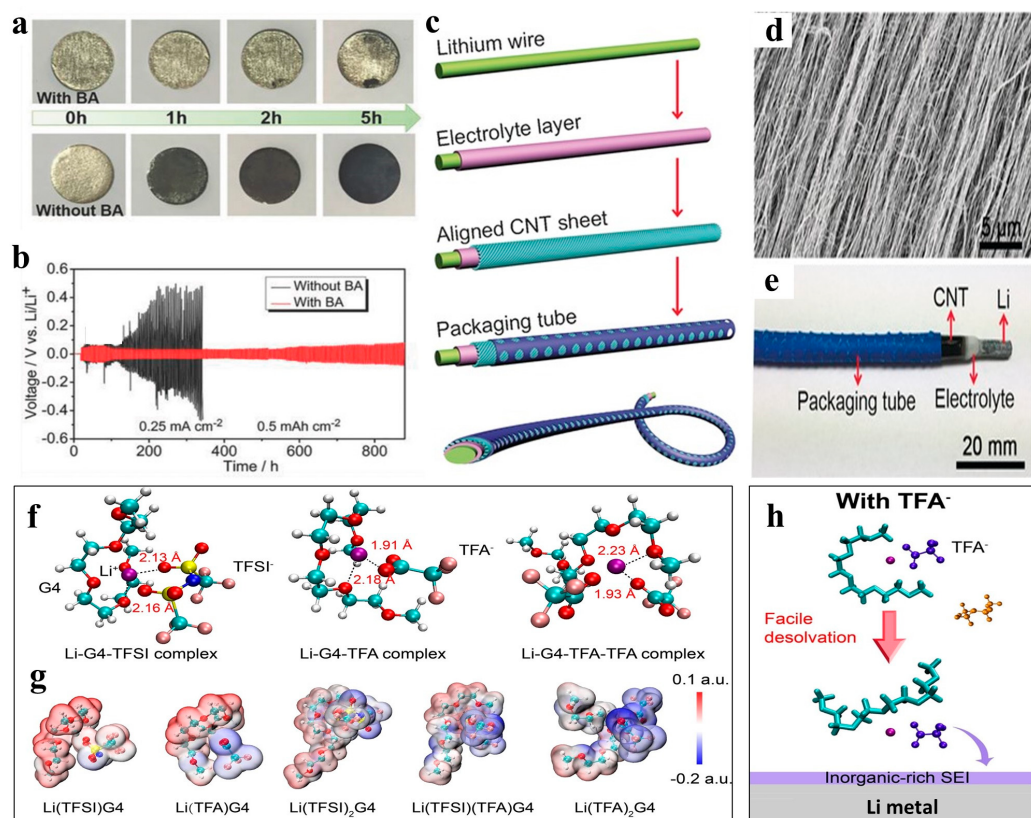


Figure 3. (a) Digital images of Li pellets with and without BA treatment after exposure to air (38 RH%) at different times. (b) Cycling performance of Li | Li symmetric cells with (red line) and without (black line) BA under O₂ atmosphere [33]. Copyright 2018, Wiley–VCH. (c) A typical fabrication. (d) SEM image of gel electrolyte coated on the Li wire. (e) Photograph of a fiber-shaped Li–air battery [34]. Copyright 2016, Wiley–VCH. (f) Optimized solvation structures in SE and BSE. (g) ESP comparison of typical solvation structures in SE and BSE. (h) Mechanism of LiTFA on the regulation of solvation structures and interfacial reactions on Li anode [35]. Copyright 2023, Wiley–VCH.

Huang et al. have developed a dual-salt electrolyte containing trifluoroacetate ions (TFA⁻) alongside lithium bis(trifluoromethanesulfonyl)imide (LiTFSI) in a G4 solvent (LiTFA/LiTFSI–G4) [35]. This electrolyte system is designed to regulate the solvation structure, therefore reducing the interaction between lithium ions and the G4 solvent. This solvation regulation strategy promotes the formation of a stable solid–electrolyte interphase (SEI) layer predominantly composed of inorganic components, which lowers the desolvation energy barrier for lithium ions and enhances interfacial kinetics. The dual-salt electrolyte strategy not only improves interfacial dynamics but also significantly enhances the cycling performance of lithium–oxygen batteries. Under conditions with a capacity-limited lithium anode (7 mAh cm⁻²), this electrolyte system extends the battery's cycle life to 120 cycles, compared to only 10 cycles achievable with a single LiTFSI/G4 electrolyte (Figure 3f–h).

Zhou et al. developed a fibrous gel polymer electrolyte (GPE) using a polyacrylonitrile (PAN) matrix through electrospinning. The 3D structure of the GPE enhances the electrolyte's absorption capacity, while its interconnected design promotes strong interactions between Li⁺ ions and the polar groups within the PAN matrix, therefore improving ion transport efficiency. In practical tests, both lithium symmetric batteries and Li–O₂ batteries demonstrated the ability to operate over long cycles at high current densities [40].

3.3. Protective Layers and Membrane Modifications

Compared to in situ generated SEI films, pre-treatment processes producing artificial protective layers are more commonly used to protect lithium anodes in lithium–oxygen batteries. A protective film for lithium anodes was developed by incorporating dextrin/β-cyclodextrin nano slurry into modified polyether ether ketone (PWC). This film features a 3D network that shields the highly reactive lithium anode from oxygen crossover [41]. A protective film composed of Al₂O₃ and PVdF-HFP demonstrated significant advantages in suppressing electrolyte decomposition and dendrite growth. After 80 cycles, batteries with protected lithium anodes exhibited discharge capacities approximately three times higher than those without any protection [42].

Park et al. fabricated ultrathin films of graphene oxide (GO) by employing a straightforward vacuum filtering technique on a porous substrate [42]. Because of their tiny dimensions, GO nanochannels preferentially permit the transit of smaller Li⁺ ions while blocking 5,10-dihydro-5,10-dimethylphenazine. Kim et al. explored phosphorene as a protective layer, which subsequently formed Li₃P through an electrochemical lithiation process [43]. The lithium plating on the lithium phosphide layer is thermodynamically unfavorable (Figure 4a–d).

Zhu et al. prepared a 30-micron-thick organic–inorganic hybrid layer by immersing Li in a mixed solution of 1-chlorodecane and cyclohexane, followed by treatment with a mixed O₂/CO₂ gas [47]. This layer serves as a barrier against Li dendrite growth, organic solvent, and dissolved oxygen corrosion. Additionally, certain special methods have been employed to protect the Li anode. Before cycling lithium–oxygen batteries in an oxygen atmosphere, electrochemical pre-treatment in pure argon gas forms an ultrathin passivation film on the lithium metal surface, further inhibiting the side reaction. Asadi et al. adopted a similar pre-treatment approach in Li–CO₂ batteries, running the battery in a pure CO₂ atmosphere to form a Li₂CO₃/C composite protective coating via the reaction between Li and CO₂ [44]. This protective layer, combined with the cathode and electrolyte, endowed the optimized lithium–oxygen battery with an ultra-long-cycle life of 700 cycles (Figure 4e–g).

Lim et al. improved the cycle stability of lithium–oxygen batteries from 65 to 130 cycles by preparing a polyethylene glycol (PEO) film on the lithium metal anode (LMA) and electrochemically precharging it in an oxygen atmosphere [45]. This process forms a polymer-supported solid–electrolyte interface (PS–SEI) layer, where inorganic components (e.g., Li₂CO₃ and LiF) are uniformly distributed within a flexible PEO matrix. This PS–SEI layer exhibits excellent mechanical and chemical properties, effectively inhibiting side reactions between the LMA and electrolyte. This method can also synergize with redox mediators (RM) to further reduce overpotential and extend the battery's cycle life (Figure 4h,i).

Chen et al. used triethylamine trihydrofluoride (TREAT–HF) as a solution and reactant to prepare a uniform, dense, continuous LiF protective layer on Li by soaking the metal and controlling the reaction temperature. This LiF layer effectively suppresses side reactions between the Li anode and electrolyte while also inhibiting dendrite growth. It demonstrated good stability in symmetric and full lithium cells. Compared to bare Li anodes, the LiF-coated anodes significantly improved corrosion resistance to humid air. Even at high current densities (4.5 mA/cm²), lithium–oxygen batteries with LiF@Li anodes maintained stable cycling for over 150 cycles with minimal polarization voltage.

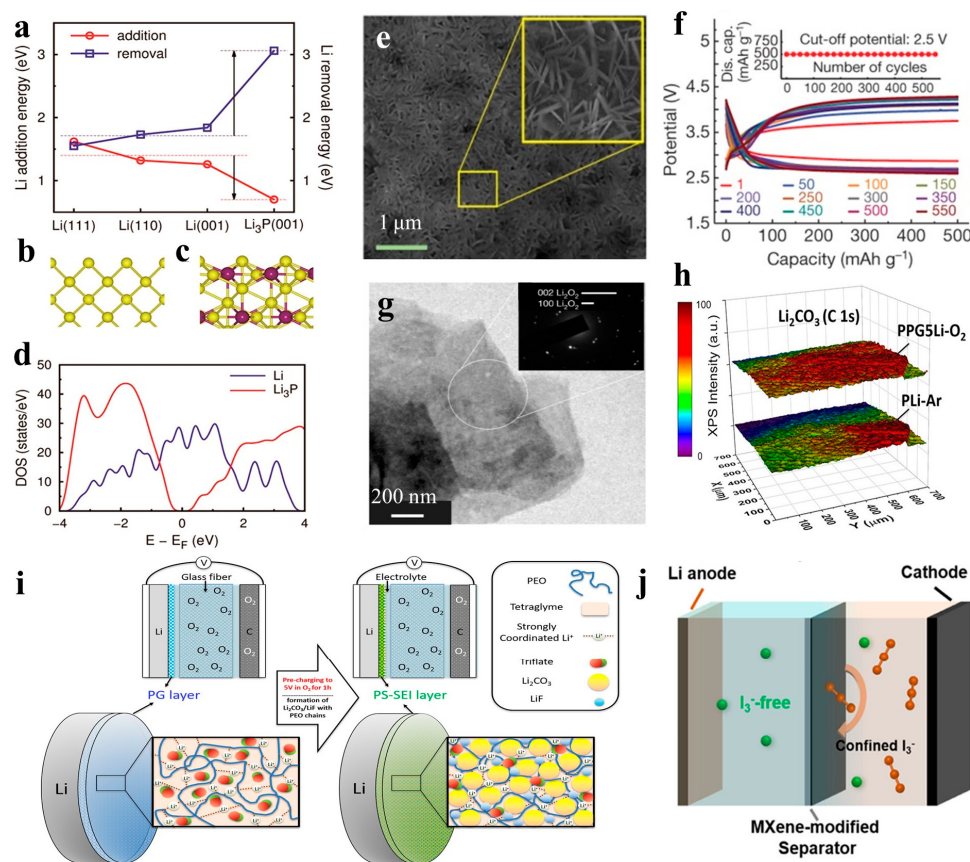


Figure 4. (a) Li addition and removal energies on Li metal and Li₃P(001) surfaces. Structures of (b) Li(001) and (c) Li₃P(001) surfaces. (d) Density of states of bcc Li metal and amorphous Li₃P. EF represents the Fermi level [43]. Copyright 2018, American Chemical Society. (e) SEM image of the protected anode surface. (f) The discharge–charge voltage profile over 550 cycles. The inset shows the capacity versus the number of cycles. (g) TEM image of a discharged cathode sample. The inset diffraction patterns show crystallinity corresponding to monoclinic lithium peroxide, Li₂O₂ [44]. Copyright 2018, Springer Nature. (h) XPS images showing the distribution of Li₂CO₃ compositions on the surface of Li metal anodes with 5 wt.% of poly(ethylene oxide) (PEO) in gel polymer (PG) from the pretreated LOB cells at 0.2 mA cm⁻² to 5 V of charge cutoff voltage under Ar or O₂ atmosphere. (i) Formation of polymer-supported solid–electrolyte interface (PS-SEI) layer on Li metal surface by electrochemical precharging to 5 V under oxygen atmosphere [45]. Copyright 2021, American Chemical Society. (j) Schematic Illustration of Suppressing I₃⁻ Shutting with the MXene–Modified Separator in Li–O₂ Batteries [46]. Copyright 2021, American Chemical Society.

Coating the separator with charged materials can effectively suppress the redox shuttle effect, and MXenes, with their rich surface functional groups, show immense potential in lithium battery applications [48,49]. Although MXenes have proven successful in mitigating the shuttle effect in lithium–iodine, lithium–sulfur, and lithium–selenium batteries, there have been no reports of their use in lithium–oxygen batteries containing redox mediators. The shuttle effect of triiodide ions (I₃⁻) severely compromises the performance of lithium–oxygen batteries, leading to the failure of redox mediators and the anode. Researchers developed a chemically bonded membrane modification strategy based on MXene, featuring a three-dimensional porous hierarchical structure [46]. The -OH functional groups abundantly present on the MXene surface effectively suppress I₃⁻ migration, while the three-dimensional porous structure ensures rapid lithium-ion transport. Li–O₂ batteries using this MXene–BC@GF membrane did not exhibit the redox mediator shuttle phenomenon during charge and discharge processes and achieved a cycle life of up to 100 cycles, three times that of the control samples. This indicates that the strategy effectively mitigates

the I_3^- shuttle effect, significantly enhancing the battery's cycling performance. This work provides new insights into developing membrane modification strategies suitable for lithium–oxygen batteries containing redox mediators (Figure 4j).

Liu et al. proposed an interface polymerization (IP)-based membrane modification method, forming a selectively permeable functional layer on the surface of a polyetherimide (PEI) membrane [50]. This functional layer is designed to inhibit the shuttle effect of large ions such as $EMIM^+$, $TFSI^-$, and BF_4^- between the electrodes while enhancing lithium-ion conductivity. Li–O₂ batteries assembled with the modified P2-PEI membrane demonstrated significantly improved performance, achieving stable operation for 135 cycles at a current density of 0.05 mA cm^{-2} and a fixed capacity of 1000 mAh g^{-1} , substantially outperforming batteries with unmodified membranes.

Furthermore, electrospinning can produce nanofibrous materials with high specific surface areas and porous structures, which enhance the electrochemical reactivity and ion transport efficiency of the electrodes in Li–O₂ batteries. Zhang et al. fabricated polyetherketone nanofiber membranes by electrospinning. These membranes exhibited excellent chemical and thermal stability, as well as mechanical strength. When used as a separator in Li–O₂ batteries, the cycle stability of the batteries significantly increased, achieving 194 cycles at 200 mA g^{-1} and 500 mAh g^{-1} [51].

4. Advances in Cathode Material Research

4.1. Progress in Cathode Material Research

The cathode is a critical component of metal–air batteries. Discharge products form on the cathode surface, and gases diffuse through the porous cathode. Consequently, cathode materials are a significant focus in metal–air battery research. Current metal–air battery cathodes typically consist of porous materials and catalysts or sometimes just one of these components. Generally, porous carbon materials serve as hosts for discharge products, while catalyst materials enhance the generation and decomposition rates of these products. Some modified carbon materials also exhibit catalytic properties, working synergistically with catalyst materials to improve the electrochemical performance of metal–air batteries.

4.1.1. Advances in Carbon-Based Cathode Materials

Porous carbon composite electrodes are predominantly used as cathodes in metal–air batteries [52]. Due to their porosity, light weight, and high conductivity, porous carbon materials (e.g., Ketjen black) and other carbon forms (e.g., graphene) are among the most promising candidates for metal–air battery cathodes [53,54]. These carbon electrodes have yielded a series of results regarding discharge products and specific capacities. Additionally, significant technological advancements in metal–air batteries have been achieved [55–57].

One of the most challenging issues is the insulation of discharge products that fill the pores of carbon air electrodes, leading to high charging overpotentials and the subsequent decomposition of the carbon cathode due to this high overpotential. Researchers are thus focused on understanding the decomposition mechanisms of carbon cathodes and the catalytic decomposition of products in metal–air batteries. McCloskey et al. first reported the instability of carbon-based cathodes in Li–O₂ batteries [58], indicating that cell potentials exceeding 4 V can lead to the decomposition of both the electrolyte and Li_2CO_3 . Additionally, intermediates such as peroxide (O_2^-) have been widely reported in recent studies. Spezia et al. revealed the degradation process of 1,2-dimethoxyethane (DME) through first-principles methods [59], investigating the reactivity of DME with superoxides in both oxygen-poor and oxygen-rich environments using density functional theory (DFT) calculations. Mahne et al. made a significant discovery, identifying the presence of singlet oxygen during the onset of discharge and charging, as well as during high-potential charging [60]. According to their findings, singlet oxygen is a primary impediment to both discharge and charge processes.

Following these results, the modification of carbon-based cathodes has garnered substantial interest. Porous nanostructuring of carbon materials has emerged as a promising

and enduring approach. In addition to structural design, research over the past few decades has explored carbon cathodes doped with elements such as nitrogen (N), sulfur (S), oxygen (O), and phosphorus (P) [61–63]. DFT simulations have shown that N,O co-doped carbon materials as cathode catalysts can alleviate the disordered growth and slow decomposition of Li_2O_2 . Specifically, porous carbon materials with high surface areas and N,O content were prepared through pyrolysis and air activation of guanosine 5'-monophosphate disodium salt (5'-GMP, 2Na) [64]. This material altered the morphology of Li_2O_2 from large toroids to films, improving battery performance. This research provides a new method for preparing high-performance porous carbon materials, aiding in the optimization of Li_2O_2 formation and decomposition processes in lithium–oxygen batteries.

Biomass-derived carbon materials are emerging as ideal cathode candidates for $\text{Li}-\text{O}_2$ batteries owing to their renewability, low cost, and environmental friendliness. These materials significantly enhance the electrical conductivity and electrochemical stability of the batteries. Zhao et al. have showcased a biomass-derived carbon material composed of bulk carbon nanosphere clusters synthesized via a low-cost, straightforward, and controllable nanoscale method [65]. The material's open, slit-like hierarchical structure offers ample active surface sites and transport channels for the electrode. Impressively, this carbon nanomaterial exhibits a high specific capacity of $20,300 \text{ mAh g}^{-1}$ and a cycling life of 543 cycles in $\text{Li}-\text{O}_2$ batteries. The synthesis method is versatile and could be able to the three main organic components of plants and biomass waste, indicating potential for large-scale application. The prepared carbon materials demonstrate excellent conductivity and electrochemical stability, with broad application prospects in energy storage, catalysts, and adsorbents (Figure 5a).

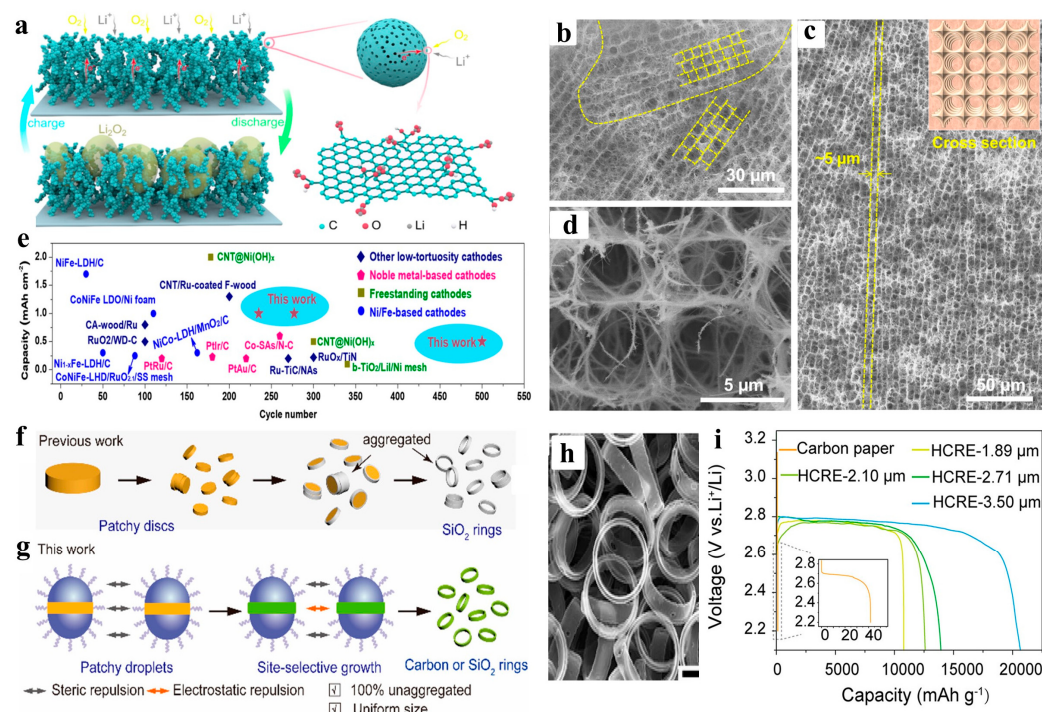


Figure 5. (a) Schematic of the cathode based on carbon nanosphere clusters in working $\text{Li}-\text{O}_2$ batteries [65]. Copyright 2021, Elsevier. (b–d) The orthogonal channels are large-area uniform distribution (c) with uniform pore size ($\sim 5 \mu\text{m}$) (d), and there are slight changes in the local mismatch of pore arrangement orientations like grain boundaries in polycrystalline materials (b). (e) Literature surveys of other low-tortuosity cathodes, Ni/Fe-based cathodes, freestanding cathodes, and noble-metal-based cathodes focus on limited areal capacity and long cycling [66]. Copyright 2023, American Chemical Society. (f,g) New strategy to obtain well-defined RF, carbon, or SiO_2 rings using patchy droplet templates. (h) SEM images of self-standing HCRE. (i) Galvanostatic discharge profiles of LOBs [67]. Copyright 2023, American Chemical Society.

Carbon nanotubes (CNTs), with their lightweight, high porosity, and large surface area, are also promising electrode materials. These characteristics enable CNTs to provide abundant active and catalytic sites, facilitating electrochemical reactions. Researchers have transformed the original randomly distributed three-dimensional CNT sponge into a low-curvature structure with regular, orthogonally interconnected channels, approximately 5 μm in lateral dimension [66]. This design effectively reduces path tortuosity, improving the kinetics of electrochemical reactions. The *in situ* growth of bifunctional transition metal hydroxide catalysts (such as NiFe(OH)_x) on the CNT surface significantly enhances battery catalytic efficiency. These catalysts address the challenges of long-cycle life and high-rate performance in Li–O₂ batteries. This CNT platform exhibits low overpotential and high areal capacity (27.5 mAh cm⁻²), achieving a cycle life of 500 cycles at a current density of 0.5 mA cm⁻². Even at a higher current density of 1 mA cm⁻², this design maintains 275 cycles, outperforming existing porous electrode materials (Figure 5b–e).

In the context of the growing demand for efficient and clean energy, porous carbon materials play a crucial role in high-performance electrode materials due to their excellent conductivity and structural tunability. Addressing this, Shi et al. introduced a novel strategy for synthesizing monodisperse carbon rings through template patch droplets, creating lithium–oxygen battery electrodes with hierarchical porous structures [67]. In this method, patch-like polystyrene (PS) discs serve as templates and hollow carbon rings are produced via a secondary templating process. These carbon rings can be directly used as self-supporting, binder-free electrodes. The study found that these carbon ring electrodes provide high discharge capacity (20,658 mAh g⁻¹), significantly enhancing the performance of lithium–oxygen batteries. This strategy is not limited to carbon ring synthesis but can also be applied to the synthesis of other materials, such as silica rings. Electrodes manufactured using this method exhibit excellent ion transport and gas diffusion performance, demonstrating substantial potential in electrocatalysis and electrochemical energy storage (Figure 5f–i).

Furthermore, Yang et al. prepared metal-free oxygen-rich carbon nanotubes (CNTs) by controlling oxidation modifications, achieving an optimized combination of electrocatalytic performance and electrical conductivity. Electrochemical results indicated that oxygen functional groups facilitate O₂ adsorption, enhancing the electrolysis of O₂ on the CNT substrate during discharge. Moreover, the oxygen groups on the oxidized CNT surfaces promoted the formation of defective Li₂O₂, which exhibited poor crystallinity and could decompose at a low charging potential of approximately 3.5 V [68].

Studies have shown that modifying carbon-based materials through defect and interface engineering can significantly enhance the electrocatalytic performance and cycling stability of batteries. Researchers have developed a metal-free N,P co-doped porous activated carbon (N,P-PAC) electrode via KOH activation and phosphorus doping. This N,P-PAC cathode demonstrated a high specific discharge capacity of 3724 mAh g⁻¹ at 100 mA g⁻¹, excellent cycling stability with up to 25 cycles at a limited capacity of 1000 mAh g⁻¹, and a low charge–discharge voltage gap of 1.22 V at 1000 mA g⁻¹. The low overpotential (EOER-ORR) of 1.54 V was also noted. The outstanding electrochemical performance of the N,P-PAC electrode is primarily attributed to its large active surface area and the oxygen-containing functional groups generated during the KOH activation and phosphorus doping processes [69].

4.1.2. Noble Metals and Their Oxides

Various noble metals (e.g., Pt, Au, Pd, Ru, Ag) and their oxides have been incorporated with conductive carbon supports. Among these, palladium and platinum have been extensively studied over recent decades and continue to attract significant research interest [70–72].

Ye et al. reported a straightforward method to prepare Pd nanodendrite structures on graphene nanosheets, which were then applied as cathode catalysts in non-aqueous Li–O₂ batteries [72]. Xu et al. described a standalone Pd-modified hollow carbon sphere deposited

on a carbon paper cathode featuring a specific porous honeycomb structure [73]. This design provided the Li–O₂ battery with high specific capacity, relatively low overpotential, and excellent rate performance. In recent years, due to their outstanding catalytic activity during the oxygen evolution reaction (OER), they have also been widely applied in Li–O₂ batteries. Zhou's group has conducted remarkable research on materials based on Ru and RuO₂, such as CNT@RuO₂, RuO₂ nanosheets, and Ru@Ni foam [74,75].

Guo et al. introduced an advancement in Li–O₂ battery research, particularly using PtIr (platinum–iridium) multibranch structures as cathode materials to enhance battery performance [76]. Density functional theory (DFT) calculations revealed that the electron transfer from iridium (Ir) to the more electronegative platinum (Pt) reduces the Lewis acidity of Pt, therefore weakening its interaction with the LiO₂ intermediate. Batteries employing the PtIr cathode demonstrated exceptional performance: the total discharge and charge overpotential was only 0.44 V, significantly lower than most other noble metal-based cathode materials. Additionally, the battery exhibited outstanding cycling stability, maintaining performance over 180 cycles with negligible degradation. In summary, this study successfully demonstrated the immense potential of PtIr multibranch structures as cathode materials for Li–O₂ batteries. This innovative design not only significantly reduces the ORR and OER overpotentials but also provides excellent cycling stability. The findings present a novel approach to designing low Lewis acidity, high-efficiency noble metal-based catalysts to enhance battery performance (Figure 6a,b).

Research indicates that the use of graphene-based cathodes in combination with iridium nanoparticles can stabilize and purify the formation of crystalline lithium superoxide (LiO₂) in batteries [77]. Specifically, researchers achieved the stabilization of the LiO₂ structure by uniformly distributing iridium nanoparticles on a graphene-based cathode, which catalyzes the reaction process. Previously, although Li–O₂ batteries had been extensively studied, none had demonstrated stability based on pure LiO₂ (Figure 6c–e).

Single-atom catalysts have been successfully applied to metal–air battery electrode materials due to their exceptional catalytic performance, thermal and chemical stability, and superior selective catalytic properties, therefore enhancing the overall performance of these batteries. In 2019, Zhou and his team pioneered the use of g-C₃N₄ nanosheet-supported Pt single atoms as cathode catalysts in lithium–oxygen batteries (LOBs), initiating research on the application of single-atom catalysts in LOBs [78]. By early 2020, the publication of two papers on the application of Co single atoms in LOBs marked a peak in research interest in single-atom catalysts for these batteries [79,80] (Figure 6f–h).

Ruthenium (Ru), as one of the platinum group metals, is known for its excellent catalytic activity and stability. Xu and his team [81] developed nitrogen-doped porous carbon materials (NC-Ru SAs) incorporating Ru single atoms as cathode materials for LOBs and conducted electrochemical performance tests. The results demonstrated that LOBs with optimized NC-3% Ru SAs as cathode catalysts exhibited a minimal overpotential of only 0.55 V (0.02 mA cm⁻²). Furthermore, *in situ* Differential Electrochemical Mass Spectrometry (DEMS) revealed an e-/O₂ ratio of only 2.14 over a complete charge–discharge cycle, indicating excellent reversibility of the battery. This study confirms the catalytic effectiveness of Ru single-atom catalysts in LOBs, highlighting their potential for significantly enhancing battery performance. Through various characterization techniques, the study shows that LiO₂ can exist stably without forming Li₂O₂. This crystalline LiO₂, produced via a novel templating mechanism, allows for repeated charge and discharge cycles at low charging potentials, significantly enhancing battery performance. This breakthrough promises to advance the development of high-energy-density batteries and opens up new applications in fields such as oxygen storage.

Wu et al. have identified the development of highly active and durable bifunctional oxygen catalysts as a crucial factor in enhancing battery performance. The researchers have demonstrated an exceptionally active and durable bifunctional electrocatalyst (Pt/RuO₂/G) by strongly anchoring Pt and RuO₂ onto graphene. The highly exposed active sites of this catalyst significantly stabilize Li–O₂ batteries. Owing to its two-dimensional porous

morphology, ultrathin thickness (approximately 2.5 nm), and the superior (110) facet formation due to spatial confinement, the Pt/RuO₂/G electrocatalyst exhibits an extremely narrow OER/ORR voltage gap of only 0.633 V [82].

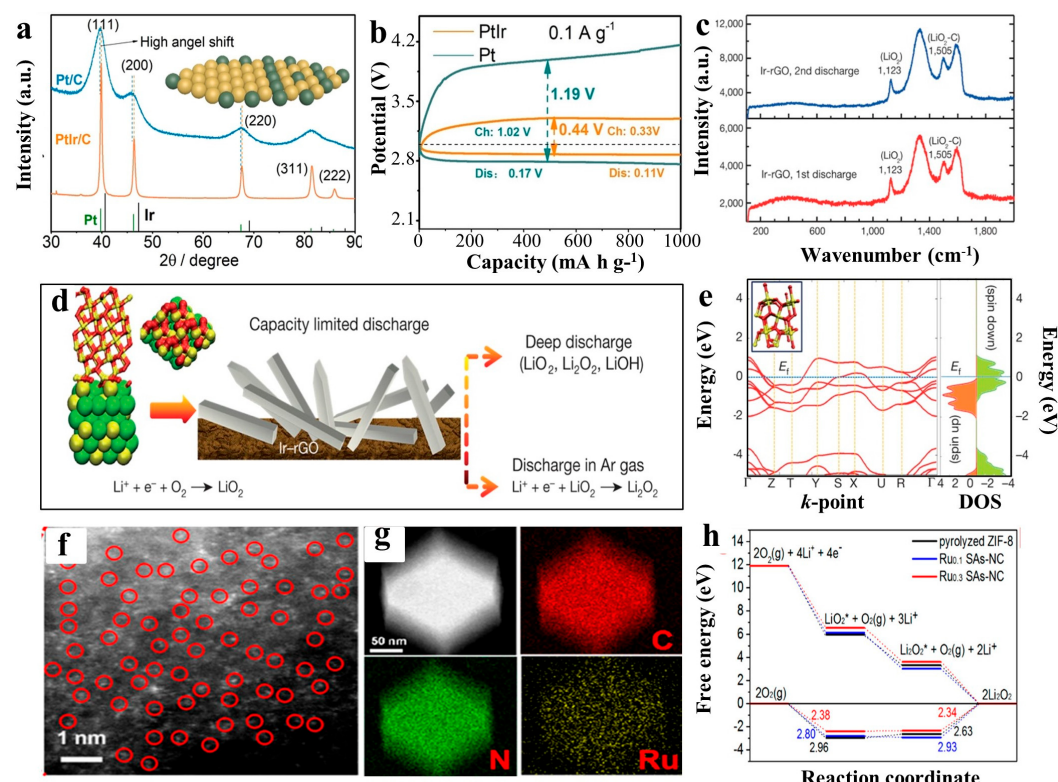


Figure 6. (a) The XRD patterns of Pt nanocrystals and PtIr multipods. (b) The galvanostatic profiles for Pt and PtIr electrodes during the discharging and charging process with a limited capacity of 1000 mAh g⁻¹ at 0.1 A g⁻¹ [76]. Copyright 2021, Wiley–VCH. (c) Raman spectra of discharge product on Ir-rGO for first and second discharges. (d) Schematic showing lattice match between Li₂O₂ and Ir₃Li that may be responsible for the Li₂O₂ discharge product found on the Ir-rGO cathode. (e) DFT electronic band structure (left) and density of states (DOS) plot (right) of ferromagnetic bulk crystalline Li₂O₂ close to the Fermi level (Ef) based on a spin-polarized calculation with electronic spin-up and spin-down states shown [77]. Copyright 2016, Springer Nature. (f) HAADF-STEM images of Ru0.3 SAs-NC (Ru single atoms are marked with red circles). (g) Corresponding EDS maps reveal the homogeneous distribution of Ru and N within the carbon support of Ru0.3 SAs-NC. (h) Gibbs free energy diagrams at 2.97 V for the discharge–charge reactions on the active surface of pyrolyzed ZIF-8, Ru0.1 SAs-NC, and Ru0.3 SAs-NC [81]. Copyright 2020, American Chemical Society.

4.1.3. Transition Metal Oxides/Carbides

While precious metals and their oxides exhibit excellent catalytic performance, their high material costs impede practical applications in Li–O₂ batteries. Therefore, it is essential to develop effective oxygen cathode catalysts for oxygen reduction (ORR) and oxygen evolution (OER) with lower costs [83]. Various non-precious metal materials, such as transition metal oxides and perovskites, have attracted considerable interest due to their outstanding oxygen electrocatalytic activity and low cost.

In 2007, P. Bruce's group compared several transition metal-based oxides (La_{0.8}Sr_{0.2}MnO₃, Fe₂O₃, Co₃O₄, CuO, NiO, CoFe₂O₄), commonly used as cathode catalysts [84–86]. In organic lithium–air battery systems, CuO, Fe₃O₄, and CoFe₂O₄ demonstrated good capacity retention, with Co₃O₄ showing the highest initial discharge capacity and capacity retention, as well as the lowest charging voltage. Subsequently, in 2008, they studied a series of manganese oxides with different crystal structures and morphologies [87]. α-MnO₂ nanowires

outperformed other manganese oxides, achieving an initial discharge capacity of up to 3000 mAh g^{-1} and excellent cycling stability (Figure 7a,b).

Due to the favorable oxygen reduction catalytic properties of manganese oxides, extensive research has been conducted on their application in lithium–air batteries [87–89]. S. Suib’s group used a one-step coprecipitation method to dope titanium into octahedral $\gamma\text{-MnO}_2$ hollow spheres, achieving a capacity of 2300 mAh g^{-1} as a cathode catalyst [90]. Zheng et al. grew $\alpha\text{-MnO}_2$ nanowires *in situ* on a graphene substrate and compared the electrochemical performance of these *in situ*-grown electrodes with mechanically mixed $\alpha\text{-MnO}_2$ nanowires and graphene [91]. The *in situ*-grown $\text{MnO}_2/\text{graphene}$ composite electrodes exhibited significantly higher charge–discharge capacities and lower overpotentials compared to the mechanically mixed electrodes. This study highlights the importance of the interaction between the catalyst and the carbon substrate in influencing catalytic activity and battery performance. Numerous studies confirm that manganese oxides significantly enhance the overall performance of lithium–air batteries, making them a popular choice for cathode catalyst research.

Recent advancements have been made in the use of transition metals and their carbides, nitrides, phosphides, and sulfides [92,93]. Molybdenum carbide (MoC_x), due to its various electronic properties and catalytic performance related to its adjustable phase composition, emerges as a promising non-precious metal catalyst. Among these, Mo_2C exhibits the best performance due to its electronic configuration near the Fermi level (EF) [94]. Efforts have been made to develop Mo_2C nanostructures with abundant active sites and composites integrating conductive substrates, such as carbon nanotubes (CNT) and graphene [95–97]. However, the negative hydrogen bonding energy (DGH^*) on Mo_2C indicates strong adsorption of H on its surface, which favors the reduction of H^+ (Volmer step) but limits its desorption (Heyrovsky/Tafel step) [94]. Therefore, optimization of electronic characteristics is necessary. Element doping has been attempted, but improvements are limited due to inadequate modification and inevitable structural damage [98]. Interface engineering, such as heterojunctions, has been explored to enhance the electrochemical performance of Mo_2C catalysts [99]. For example, $\text{Mo}_2\text{N}-\text{Mo}_2\text{C}$ heterojunctions are efficient hydrogen evolution catalysts [100], showing superior catalytic activity compared to Pt/C at high current densities ($>88 \text{ mA cm}^{-2}$) in alkaline media.

Two-dimensional transition metal carbides/nitrides, known as MXenes, exhibit significant potential as catalysts in Li-O_2 batteries due to their unique layered structures and excellent conductivity [101]. However, further enhancement of their catalytic performance remains a focus of research. Researchers prepared nitrogen-doped Ti_3C_2 MXene catalysts using hydrothermal and annealing methods, resulting in increased disorder and abundant active sites. Density functional theory (DFT) calculations indicated that nitrogen doping adjusted the occupation of Ti 3d orbitals in N-Ti₃C₂(H), enhancing the electron exchange between Ti 3d orbitals and O 2p orbitals, thus accelerating oxygen electrode reactions. Li-O_2 batteries based on N-Ti₃C₂(H) exhibited a large discharge capacity of $11,679.8 \text{ mAh g}^{-1}$ and stable cycling performance over 372 cycles. *In situ* Differential Electrochemical Mass Spectrometry (DEMS) confirmed the effective accumulation and decomposition of Li_2O_2 on the N-Ti₃C₂(H) surface. This study proposed a valuable strategy to boost oxygen electrode reaction catalytic activity by tuning the 3d orbital occupation in MXenes, highlighting the potential of nitrogen-doped Ti_3C_2 MXene for high-performance Li-O_2 batteries (Figure 7c).

Yang et al. investigated the activity of Li-O_2 batteries by constructing adsorption models of Li_xO_2 ($x = 4, 2, 1$) on Ti_2C -MXene with different functional groups (-O, -F, -OH) [102]. Their computational results indicated that Ti_2CO_2 MXene exhibits superior catalytic activity, with an ORR overpotential of 0.10 V and an OER overpotential of 0.16 V. The polarization of the Ti 3d orbitals near the Fermi level determines the reducibility of Ti_2C MXene, directly influencing the oxidation reaction of O_2 (Figure 7d–f).

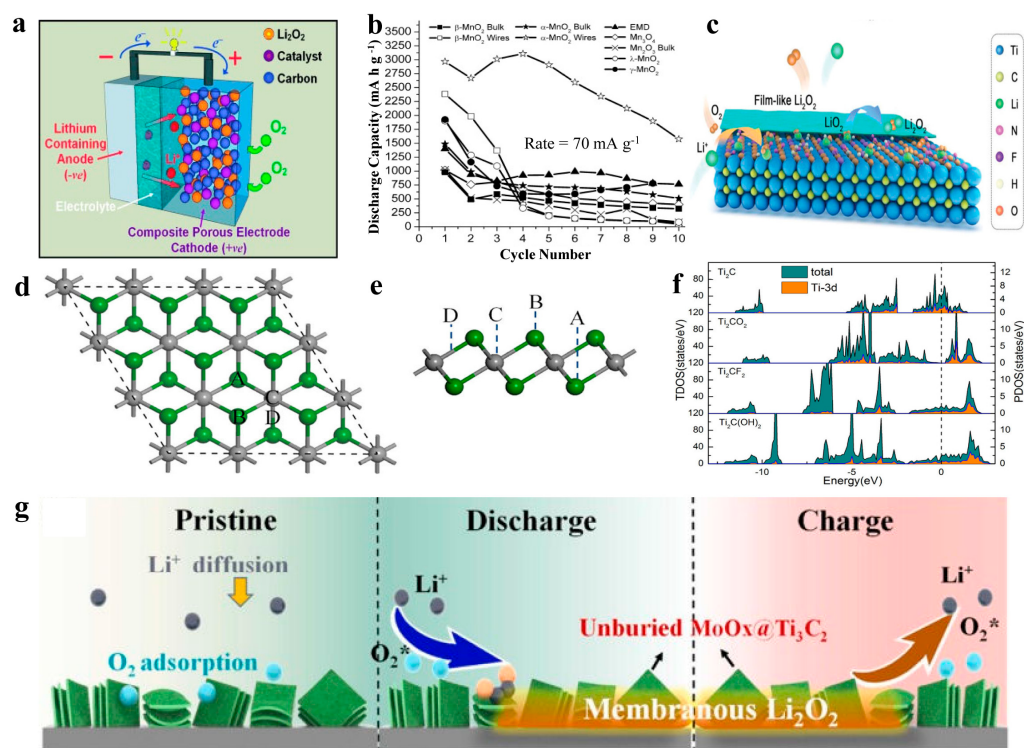


Figure 7. (a) Schematic representation of a rechargeable Li/O₂ battery. (b) Variation of discharge capacity with cycle number for several porous Mn-based [87]. Copyright 2008, Wiley–VCH. (c) The schematic diagram of the formation and decomposition of discharge product Li₂O₂ on the N-Ti₃C₂(H) surface during the discharge and charge process, respectively [101]. Copyright 2023, Wiley–VCH. Top (d) and side (e) views of the Ti₂C MXene monolayer. The capitals in the figure are the possible adsorption sites. Green and gray atoms are Ti and C, respectively. (f) Calculated total density of states (left) and projected density of states of Ti 3d (right) for Ti₂C, Ti₂CO₂, Ti₂CF₂, and Ti₂C(OH)₂. The vertical dashed line at E = 0 eV represents the Fermi energy [102]. Copyright 2019, American Chemical Society. (g) Schematic diagram of the reaction during the cycling process in LOBs (* represents adsorptive state). [103]. Copyright 2021, Elsevier.

Recently, Li et al. obtained similar results through both experimental and theoretical calculations. They used thermally treated Ti₂C MXene nanosheets with surface -O and -F functional groups as cathode catalysts for Li-O₂ batteries. At a current density of 100 mA g⁻¹, the discharge capacity reached 15,635 mAh g⁻¹. At a current density of 200 mA g⁻¹, a fixed capacity of 600 mAh g⁻¹ was maintained over 250 cycles, demonstrating long-cycle stability. Computational results showed that Ti₂CO₂ has the most suitable adsorption strength for Li₂O₂, outperforming Ti₂CF₂ and bare Ti₂C in catalytic performance. Due to surface heterogeneity, discharge products primarily nucleate at Ti₂CO₂ sites during the discharge process and accumulate spatially to form a porous structure, effectively promoting mass transfer and cyclic stability.

Despite their optimized charge density and extended electronic properties, MXenes tend to oxidize and restack under high anodic potentials. Molybdenum oxides, with their multiple valence states and high electronegativity, show potential for ORR/OER catalysis [104]. Nitrogen-doped MoO₂ can enhance LiO₂ adsorption and promote uniform growth of Li₂O₂. Mo-based compounds can form heterojunctions, accelerating charge distribution and improving chemical stability. Sun et al. achieved strong self-assembly of MoO_x and Ti₃C₂ MXene, creating a novel stable bimetallic Mo/Ti-O coupled catalyst with optimized interfacial electronic structure, high chemical stability, and enhanced ORR/OER bifunctional activity. Experimental results showed that Li-O₂ batteries with MoO_x@Ti₃C₂ MXene cathodes exhibited lower voltage polarization, longer lifespan, and superior rate performance compared to other monoclinic catalysts. Experimental and theoretical analyses

further revealed the crucial impact of bimetallic–oxygen coupling in promoting ORR/OER kinetics and optimizing Li_2O_2 adsorption/desorption (Figure 7g).

Studies have demonstrated that the rational design and adjustment of the structure and morphology of catalytic cathode materials can effectively optimize battery performance. Xu et al. designed a three-dimensional open-structured $\text{Co}_3\text{O}_4@\text{MnO}_2$ heterojunction composite material through a simple two-step hydrothermal method [105]. This composite, serving as a bifunctional catalyst and featuring a three-dimensional open structure, guides the uniform and fluffy deposition of discharge products like Li_2O_2 . When used as a cathode for Li–O₂ batteries, it exhibits excellent electrochemical performance, including an initial discharge-specific capacity as high as 12,980 mAh g⁻¹.

4.1.4. Perovskite Materials

To date, perovskite-based composite oxides (ABO_3) have emerged as promising alternatives to noble metal bifunctional catalysts in lithium–oxygen (Li–O₂) batteries due to their significantly lower cost, excellent catalytic activity and high oxygen mobility. Various perovskites such as $\text{Sr}_{0.95}\text{Ce}_{0.05}\text{CoO}_{3-x}$, $\text{La}_{0.8}\text{Sr}_{0.2}\text{MnO}_3$, and $\text{Sr}_2\text{CrMoO}_{6-x}$ have been utilized in Li–O₂ batteries [106–108]. However, perovskite catalyst materials synthesized by conventional methods often exhibit low intrinsic electronic conductivity and small specific surface areas, which limit their catalytic activity and practical application.

Additionally, synthesizing perovskites with porous structures that offer efficient oxygen pathways and high specific surface areas has been pursued to boost catalytic performance. For example, Zhang et al. reported the use of 3D ordered macroporous (3DOM) LaFeO_3 and $\text{La}_{0.75}\text{Sr}_{0.25}\text{MnO}_3$ nanotubes (PNT–LSM) [109,110] (Figure 8a,b). These porous nanotubes consist of nanoparticles with typical sizes ranging from 10 to 30 nm. When first used as electrocatalysts in Li–O₂ batteries, PNT–LSM significantly suppressed the overpotentials for oxygen reduction (ORR) and particularly oxygen evolution (OER), therefore improving round-trip efficiency. The high catalytic activity of PNT–LSM and the synergistic effects of their unique hollow channel structure endowed the Li–O₂ batteries with high specific capacities, excellent rate capabilities, and good cycling stability (Figure 8c,d).

Typical perovskite oxides like LaMO_3 (M = Mn, Fe, Co, Ni) have garnered wide attention. Oxygen defect engineering and morphology control are forward-looking strategies to address these issues. Regulating oxygen vacancies can accelerate electron transport and reduce reaction energy barriers, while oxygen vacancies also serve as efficient sites to promote the binding and decomposition of intermediate and discharge products like Li_2O_2 . Morphology and surface structure significantly influence catalytic efficiency, with optimal surface structures providing more active sites to facilitate electrochemical reactions. Scientists have suggested a combined approach of flaw and surface engineering, where oxygen vacancies are regulated on the surface of $\text{LaCo}_x\text{Mn}_{1-x}\text{O}_{3-\sigma}$, and cation substitution is achieved via a template-free growth method to optimize morphology, therefore enhancing electrocatalytic performance. It was found that $\text{LaCo}_{0.75}\text{Mn}_{0.25}\text{O}_{3-\sigma}$ exhibited the best electrochemical performance among all candidate materials. Its unique porous hollow structure and rough surface nanosheets increased active site accessibility, promoted mass transfer, and enhanced catalytic performance (Figure 8e–g). This catalyst demonstrated a low overpotential (only 1.12 V), a high initial specific capacity (up to 10,301 mAh g⁻¹), and a stable cycling life [111].

Additionally, researchers have employed $\text{LaNi}_{0.5}\text{Co}_{0.5}\text{O}_3$ (LNCO) as a bifunctional catalyst and cathode substrate for Li–O₂ batteries, eliminating the need for carbon materials [112]. In a molten nitrate electrolyte at 160 °C, LNCO exhibited an ultra-low charge-discharge overpotential of 50 mV, an energy efficiency of up to 98.2%, and remained stable for over 100 cycles at a current density of 0.1 mA/cm². These demonstrated long-term cycling stability and efficient operation. Density functional theory (DFT) calculations confirmed the electronic structure and excellent catalytic activity of LNCO. The study highlighted LNCO's semimetal characteristics and the coexistence of surface $\text{Ni}^{2+}/\text{Ni}^{3+}$ and $\text{Co}^{2+}/\text{Co}^{3+}$ redox pairs, effectively catalyzing both ORR and OER reactions. For the

first time, porous and fluffy Li_2O was identified as the discharge product, and a detailed four-electron transfer mechanism was proposed (Figure 8h–j).

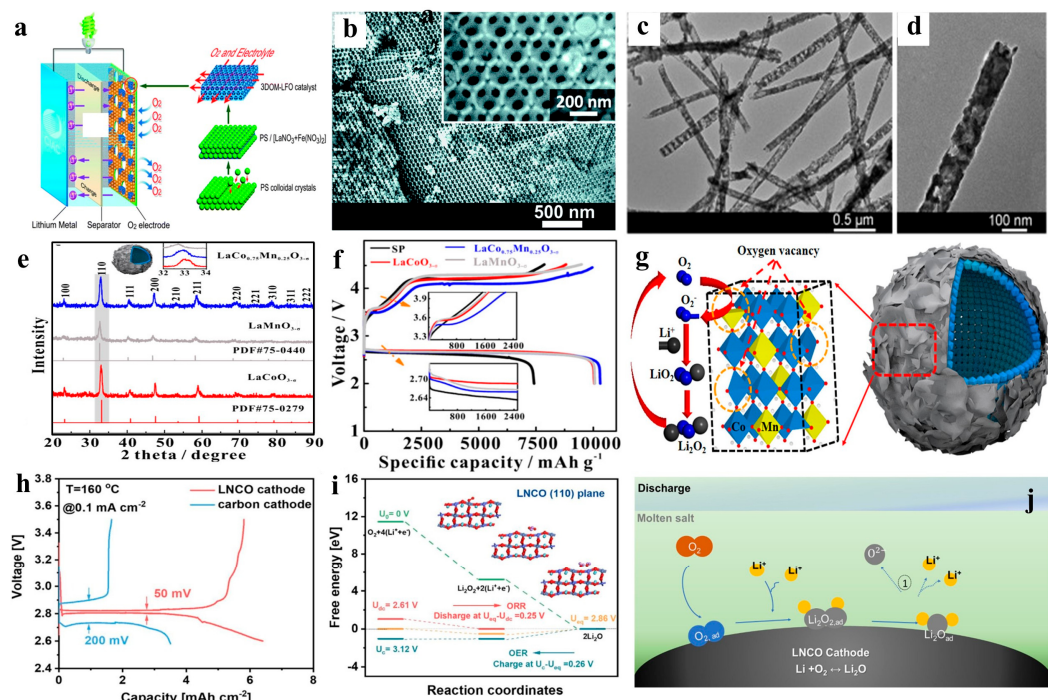


Figure 8. (a) Schematic illustration for preparation of 3DOM-LFO catalyst and structure of the rechargeable $\text{Li}-\text{O}_2$ batteries. (b) FESEM images of 3DOM-LFO after calcination at $600\text{ }^\circ\text{C}$ for 3 h. Inset in (a): magnified FESEM image [109]. Copyright 2014, The Royal Society of Chemistry. (c) Low- and (d) High-magnification TEM images of PNT-LSM [110]. Copyright 2013, Wiley-VCH. (e) XRD patterns of $\text{LaCo}_x\text{Mn}_{1-x}\text{O}_{3-\sigma}$ ($x = 1, 0.75$, and 0) samples. (f) $\text{Li}-\text{O}_2$ batteries with SP and $\text{LaCo}_x\text{Mn}_{1-x}\text{O}_{3-\sigma}$ electrode ($x = 1, 0.75$, and 0) for (a) galvanostatic discharge/charge curves at a current density of 200 mA g^{-1} . (g) Mechanism of oxygen vacancy for ORR/OER processes occurring on the surface of $\text{LaCo}_{0.75}\text{Mn}_{0.25}\text{O}_{3-\sigma}$ catalyst during charging/discharging in $\text{Li}-\text{O}_2$ Battery [111]. Copyright 2020, American Chemical Society. (h) Full discharge and charge curves of the cell with LNCO cathode (red curves) and with SPC cathode (blue curves). (i) Gibbs free energy diagrams of the LNCO electrode reactions. The insets are the optimized structures of the LNCO (1 1 0) with adsorbates at corresponding discharging steps. (j) Schematic illustration of the discharge pathway on the LNCO cathode surface [112]. Copyright 2023, Elsevier.

4.1.5. Emerging Cathode Materials

In the realm of lithium–oxygen ($\text{Li}-\text{O}_2$) battery research, traditional catalysts often face limitations due to low activity and instability. High-entropy alloys (HEAs), composed of multiple metal elements, exhibit unique properties such as lattice distortion effects, sluggish diffusion, and the “cocktail effect,” which show considerable potential in electrocatalysis and rechargeable batteries. These alloys optimize electron transfer and intermediate adsorption energies through the synergistic effects of multiple metals, therefore lowering redox barriers (Figure 9a–c).

Guo et al. have developed an innovative synthesis method using silver nanowires (Ag NWs) as templates to create ultrathin 2D high-entropy alloy subnanometer ribbons (SNRs) with up to eight metal elements and a layer thickness of just 0.8 nm , the thinnest HEA reported to date [113]. This method includes extensive metal exchange reactions, co-reduction, and the removal of the core silver. Pentanary HEA (PtPdIrRuAg) SNRs exhibited exceptional mass activity for the ORR in alkaline electrolytes, surpassing commercial Pt/C catalysts by 21 times. Hexanary HEA (PtPdIrRuAuAg) SNRs demonstrated low charge overpotentials (0.49 V) and excellent cycle life (100 cycles) in $\text{Li}-\text{O}_2$ batteries. Density

functional theory (DFT) calculations and molecular dynamics (MD) simulations have been used to study the structural changes and atomic arrangements of HEA SNRs, with electronic structure analyses revealing a balance between metal selection, composition, and the number of elements contributing to their electrocatalytic activity and stability.

Developing HEAs with spatial heterostructures to manipulate the d-band center of interfacial metal atoms and adjust electronic distributions is an essential challenge and fundamental research direction to enhance HEA catalyst electrocatalytic activity. By growing uniform Pt dendritic structures on a PtRuFeCoNi HEA core, a unique HEA@Pt spatial heterostructure electrocatalyst was constructed. This structure aids in accelerating ORR and OER kinetics [114]. Theoretical calculations indicated that the electron redistribution at the interface regulated the d-band center of metal atoms, optimizing oxygen species adsorption energy and reducing ORR/OER reaction barriers. This charge transfer and redistribution improved the electrocatalytic activity and cycling performance of the catalyst. Li–O₂ batteries based on HEA@Pt electrocatalysts exhibited low polarization potential (0.37 V) and long-term cycling stability (210 cycles) at a cutoff capacity of 1000 mAh g⁻¹, outperforming most previous noble metal catalysts. Additionally, HEA@Pt demonstrated excellent catalytic activity and stability in alkaline media, indicating its significant potential in a wide range of catalytic applications.

The Sabatier Principle, proposed by French chemist Paul Sabatier, is a guiding theory for designing and selecting heterogeneous catalysts. It has broad applications in various chemical reactions, including hydrogenation, ammonia synthesis, and water–gas shift reactions. In fuel cells, industrial chemical reactions, and the latest electrocatalyst research, such as Li–O₂ batteries, it guides the selection of effective catalysts. Based on the Sabatier Principle, researchers have systematically used high-entropy strategies to construct a series of catalysts with widely distributed d-band centers (i.e., a wide range of adsorption strengths), uncovering the Sabatier relationship in electrocatalysts for Li–O₂ batteries [115]. A Li–O₂ battery using FeCoNiMnPtIr (HEAPtIr) as the catalyst demonstrated over 80% energy conversion efficiency and stable operation for 2000 h at a fixed specific capacity of 4000 mAh g⁻¹. This study confirmed the applicability of the Sabatier Principle in designing advanced heterogeneous catalysts for Li–O₂ batteries, providing insightful guidance for HEA catalyst design (Figure 9d–f).

Metal–organic frameworks (MOFs) offer high specific surface areas and adjustable structures, providing numerous dispersed active sites, making them promising candidates for improving catalytic efficiency and reaction rates in Li–O₂ battery cathodes. By designing different metals and ligands, MOFs can flexibly optimize battery performance and enhance electron and ion transport efficiency. Additionally, their ordered structures and high stability contribute to improved cycling life and overall performance of Li–O₂ batteries. For instance, synthesizing a single-crystal MOF with PbO₇ nodes (naphthalene-lead-MOF, known as Na–Pb–MOF) significantly improved the kinetics of discharge and charge processes in Li–O₂ batteries [116]. Compared to traditional PbO₆ nodes, the increased Pb–O bond length in PbO₇ nodes weakens orbital coupling, optimizing the adsorption of intermediate LiO₂, reducing activation energies for LiO₂ reduction to Li₂O₂ and LiO₂ oxidation to O₂, and therefore lowering the overall reaction overpotential. Consequently, Li–O₂ batteries with Na–Pb–MOF electrocatalysts exhibited a low total discharge–charge overpotential (0.52 V) and superior cycling performance, maintaining stability for 140 cycles. Additionally, solvothermal or in situ construction methods can precisely control MOF crystal growth and metal node distribution, further optimizing catalytic performance and cycling life of Li–O₂ batteries presenting new directions for electrocatalyst design (Figure 9g,h).

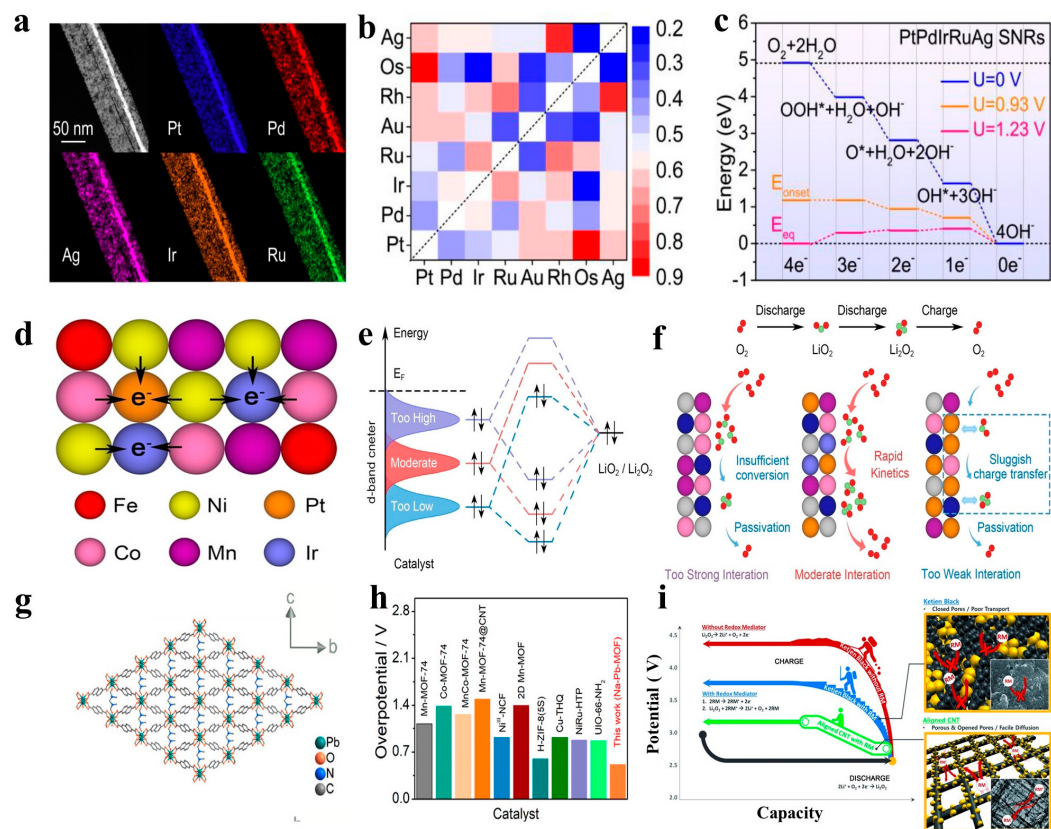


Figure 9. (a) HAADF-STEM image and EDS element mapping images of one segment of an HEA-PtPdIrRuAg SNR. Pt (blue), Pd (red), Ag (magenta), Ir (orange), and Ru (green) signals. (b) Possibility of an atomic pair in different HEAs. The color bar represents the possibility of the bonding between different metals, which ranges from 0 to 1. (c) ORR performances of quinary PtPdIrRuAg SNRs [113]. Copyright 2023, American Chemical Society. (d) Schematic diagram of electron transfer in HEAPtIr. (e) Orbital interactions between $\text{LiO}_2/\text{Li}_2\text{O}_2$ and catalysts with different d-band centers and (f) the corresponding catalytic effects [115]. Copyright 2023, Wiley-VCH. (g) The single-crystal structure of Na-Pb-MOF. (h) Comparison of overall overpotentials of Na-Pb-MOF and the reported MOF-based electrocatalysts [116]. Copyright 2023, American Chemical Society. (i) Schematic illustration of the role of the redox mediator (RM) in a Li-O₂ battery system made using a hierarchical CNT fibril electrode [32]—copyright 2014, Wiley-VCH.

Efficient catalysts are crucial for improving Li-O₂ battery performance [117]. Although solid-state catalysts have demonstrated excellent electrocatalytic performance, their complex preparation methods and limited active sites hinder large-scale application. In contrast, soluble catalysts (e.g., ORR and OER catalysts) uniformly distributed in the electrolyte can better contact reactants, reduce discharge/charge overpotentials, and improve battery cycling performance. Lim et al. demonstrated a novel lithium–oxygen battery that achieved high reversibility and good energy efficiency using a layered nanoporous air electrode and soluble LiI. This design delivered a reversible capacity of 1000 mAh g^{-1} and sustained 900 cycles with reduced polarization. The future development of lithium–oxygen batteries will require the synergistic integration of multiple technological elements to achieve overall performance enhancement (Figure 9i). Zhou et al. adopted an organometallic soluble catalyst, tris(acetylacetone)iridium [$\text{Ir}(\text{acac})_3$], whose multivalent metal active centers can capture O_2^- to form intermediate complexes ($\text{Ir}(\text{acac})_3\text{-O}_2^-$), effectively modulating ORR and OER pathways while suppressing side reactions caused by oxygen radicals. $\text{Ir}(\text{acac})_3$, by forming reversible intermediate complexes ($\text{Ir}(\text{acac})_3\text{-O}_2^-$), prolonged the diffusion time of superoxide radicals during discharge, enhancing the solution-based ORR mechanism and mitigating cathode passivation [32]. During charging, $\text{Ir}(\text{acac})_3$ acted as a redox me-

diator, accelerating Li_2O_2 decomposition, reducing charge overpotential, and effectively inhibiting singlet oxygen (${}^1\text{O}_2$) formation. Experimental results showed that Li– O_2 batteries containing $\text{Ir}(\text{acac})_3$ exhibited low overpotential, high discharge capacity, large capacity, and good stability (130 cycles). This study demonstrated a new approach to enhancing Li– O_2 battery performance by developing multifunctional soluble catalysts, indicating the need to further explore alternative catalysts to improve overall battery efficiency.

5. Summary and Outlook

This review presented the latest advances in anode and cathode materials for lithium–oxygen batteries, emphasizing their significant potential for high-energy-density applications. Research on anode materials has explored alternatives to pure lithium metal, such as silicon and lithium-rich alloys, to improve stability and mitigate dendrite formation. The development of durable solid–electrolyte interfaces (SEI) and innovative alloy compositions has shown promise in enhancing cycling stability. On the cathode side, the focus has been on improving the ORR and OER kinetics through advanced carbon-based materials and bifunctional catalysts. These advancements address the accumulation of discharge products and high overpotentials, leading to improved electrochemical performance.

The future development of Li– O_2 batteries will concentrate on refining electrode materials, optimizing pore structures, and enhancing electrolyte stability. By addressing these challenges, Li– O_2 batteries could become a viable solution for high-energy storage, combining low costs, high specific capacity, and good durability, making them promising candidates for environmentally friendly energy devices.

Author Contributions: Writing—original draft preparation, J.G. and X.M.; writing—review and editing, S.L., Q.W. and Y.Z.; visualization, J.G., X.M. and S.Y. All authors have read and agreed to the published version of the manuscript.

Funding: This work was financially supported by the National Natural Science Foundation of China (No. 52304325), the Natural Science Foundation—Chunhui Talent Project Foundation of Hebei Province (E2023501016), the Fundamental Research Funds for the Central Universities (N2323013).

Institutional Review Board Statement: This study did not require ethical approval.

Informed Consent Statement: This study is not involving humans.

Data Availability Statement: Data are available on request.

Conflicts of Interest: The authors declare no conflict of interest. The funders had no role in the design of the study, in the collection, analyses, or interpretation of data, in the writing of the manuscript, or in the decision to publish the results.

References

- Chi, X.; Li, M.; Di, J.; Bai, P.; Song, L.; Wang, X.; Li, F.; Liang, S.; Xu, J.; Yu, J. A Highly Stable and Flexible Zeolite Electrolyte Solid-State Li–Air Battery. *Nature* **2021**, *592*, 551–557. [[CrossRef](#)] [[PubMed](#)]
- Zubi, G.; Dufó-López, R.; Carvalho, M.; Pasaoglu, G. The Lithium-Ion Battery: State of the Art and Future Perspectives. *Renew. Sustain. Energy Rev.* **2018**, *89*, 292–308. [[CrossRef](#)]
- Thackeray, M.M.; Wolverton, C.; Isaacs, E.D. Electrical Energy Storage for Transportation—Approaching the Limits of, and Going beyond, Lithium-Ion Batteries. *Energy Environ. Sci.* **2012**, *5*, 7854. [[CrossRef](#)]
- Kim, T.; Song, W.; Son, D.-Y.; Ono, L.K.; Qi, Y. Lithium-Ion Batteries: Outlook on Present, Future, and Hybridized Technologies. *J. Mater. Chem. A* **2019**, *7*, 2942–2964. [[CrossRef](#)]
- Lu, T.; Qian, Y.; Liu, K.; Wu, C.; Li, X.; Xiao, J.; Zeng, X.; Zhang, Y.; Chou, S. Recent Progress of Electrolyte Materials for Solid-State Lithium–Oxygen (Air) Batteries. *Adv. Energy Mater.* **2024**, *14*, 2400766. [[CrossRef](#)]
- Rigoni, A.S.; Breedon, M.; Spencer, M.J.S. Use of Perfluorochemicals in Li–Air Batteries: A Critical Review. *ACS Appl. Mater. Interfaces* **2024**, *16*, 26967–26983. [[CrossRef](#)] [[PubMed](#)]
- Wang, G.; Yang, Y.; Zhang, Q.; Xie, Z.; Zhou, Z. Graphitic Carbon Nitride ($\text{g}-\text{C}_3\text{N}_4$) Based Photo-Assisted Li– O_2 Batteries: Progress, Challenge, and Perspective. *Coord. Chem. Rev.* **2024**, *511*, 215879. [[CrossRef](#)]
- Ge, B.; Hu, L.; Yu, X.; Wang, L.; Fernandez, C.; Yang, N.; Liang, Q.; Yang, Q. Engineering Triple-Phase Interfaces around the Anode toward Practical Alkali Metal–Air Batteries. *Adv. Mater.* **2024**, *36*, 2400937. [[CrossRef](#)] [[PubMed](#)]

9. Geng, D.; Ding, N.; Hor, T.S.A.; Chien, S.W.; Liu, Z.; Wuu, D.; Sun, X.; Zong, Y. From Lithium-Oxygen to Lithium-Air Batteries: Challenges and Opportunities. *Adv. Energy Mater.* **2016**, *6*, 1502164. [[CrossRef](#)]
10. Jung, J.-W.; Cho, S.-H.; Nam, J.S.; Kim, I.-D. Current and Future Cathode Materials for Non-Aqueous Li-Air (O_2) Battery Technology—A Focused Review. *Energy Storage Mater.* **2020**, *24*, 512–528. [[CrossRef](#)]
11. Kumar, J.; Kumar, B. Development of Membranes and a Study of Their Interfaces for Rechargeable Lithium-Air Battery. *J. Power Sources* **2009**, *194*, 1113–1119. [[CrossRef](#)]
12. Chang, Z.; Xu, J.; Liu, Q.; Li, L.; Zhang, X. Recent Progress on Stability Enhancement for Cathode in Rechargeable Non-Aqueous Lithium-Oxygen Battery. *Adv. Energy Mater.* **2015**, *5*, 1500633. [[CrossRef](#)]
13. Wang, K.; Zhu, Q.; Chen, J. Strategies toward High-Performance Cathode Materials for Lithium-Oxygen Batteries. *Small* **2018**, *14*, 1800078. [[CrossRef](#)] [[PubMed](#)]
14. Cheng, F.; Chen, J. Metal-Air Batteries: From Oxygen Reduction Electrochemistry to Cathode Catalysts. *Chem. Soc. Rev.* **2012**, *41*, 2172. [[CrossRef](#)] [[PubMed](#)]
15. Shao, Y.; Ding, F.; Xiao, J.; Zhang, J.; Xu, W.; Park, S.; Zhang, J.; Wang, Y.; Liu, J. Making Li-Air Batteries Rechargeable: Material Challenges. *Adv. Funct. Mater.* **2013**, *23*, 987–1004. [[CrossRef](#)]
16. Xu, K.; Von Cresce, A. Interfacing Electrolytes with Electrodes in Li Ion Batteries. *J. Mater. Chem.* **2011**, *21*, 9849. [[CrossRef](#)]
17. Shu, C.; Wang, J.; Long, J.; Liu, H.; Dou, S. Understanding the Reaction Chemistry during Charging in Aprotic Lithium-Oxygen Batteries: Existing Problems and Solutions. *Adv. Mater.* **2019**, *31*, 1804587. [[CrossRef](#)] [[PubMed](#)]
18. Hirshberg, D.; Sharon, D.; De La Llave, E.; Afri, M.; Frimer, A.A.; Kwak, W.-J.; Sun, Y.-K.; Aurbach, D. Feasibility of Full (Li-Ion)- O_2 Cells Comprised of Hard Carbon Anodes. *ACS Appl. Mater. Interfaces* **2017**, *9*, 4352–4361. [[CrossRef](#)]
19. Deng, H.; Qiu, F.; Li, X.; Qin, H.; Zhao, S.; He, P.; Zhou, H. A Li-Ion Oxygen Battery with Li-Si Alloy Anode Prepared by a Mechanical Method. *Electrochim. Commun.* **2017**, *78*, 11–15. [[CrossRef](#)]
20. Hassoun, J.; Jung, H.-G.; Lee, D.-J.; Park, J.-B.; Amine, K.; Sun, Y.-K.; Scrosati, B. A Metal-Free, Lithium-Ion Oxygen Battery: A Step Forward to Safety in Lithium-Air Batteries. *Nano Lett.* **2012**, *12*, 5775–5779. [[CrossRef](#)] [[PubMed](#)]
21. Kwak, W.-J.; Shin, H.-J.; Reiter, J.; Tsiovaras, N.; Hassoun, J.; Passerini, S.; Scrosati, B.; Sun, Y.-K. Understanding Problems of Lithiated Anodes in Lithium Oxygen Full-Cells. *J. Mater. Chem. A* **2016**, *4*, 10467–10471. [[CrossRef](#)]
22. Wu, S.; Zhu, K.; Tang, J.; Liao, K.; Bai, S.; Yi, J.; Yamauchi, Y.; Ishida, M.; Zhou, H. A Long-Life Lithium Ion Oxygen Battery Based on Commercial Silicon Particles as the Anode. *Energy Environ. Sci.* **2016**, *9*, 3262–3271. [[CrossRef](#)]
23. Lökçü, E.; Anik, M. Synthesis and Electrochemical Performance of Lithium Silicide Based Alloy Anodes for Li-Ion Oxygen Batteries. *Int. J. Hydrogen Energy* **2021**, *46*, 10624–10631. [[CrossRef](#)]
24. Elia, G.A.; Bresser, D.; Reiter, J.; Oberhumer, P.; Sun, Y.-K.; Scrosati, B.; Passerini, S.; Hassoun, J. Interphase Evolution of a Lithium-Ion/Oxygen Battery. *ACS Appl. Mater. Interfaces* **2015**, *7*, 22638–22643. [[CrossRef](#)] [[PubMed](#)]
25. Guo, Z.; Dong, X.; Wang, Y.; Xia, Y. A Lithium Air Battery with a Lithiated Al-Carbon Anode. *Chem. Commun.* **2015**, *51*, 676–678. [[CrossRef](#)] [[PubMed](#)]
26. Chen, Y.; Freunberger, S.A.; Peng, Z.; Bardé, F.; Bruce, P.G. Li- O_2 Battery with a Dimethylformamide Electrolyte. *J. Am. Chem. Soc.* **2012**, *134*, 7952–7957. [[CrossRef](#)] [[PubMed](#)]
27. Chen, Y.; Freunberger, S.A.; Peng, Z.; Fontaine, O.; Bruce, P.G. Charging a Li- O_2 Battery Using a Redox Mediator. *Nat. Chem.* **2013**, *5*, 489–494. [[CrossRef](#)] [[PubMed](#)]
28. Bryantsev, V.S.; Giordani, V.; Walker, W.; Uddin, J.; Lee, I.; Van Duin, A.C.T.; Chase, G.V.; Addison, D. Investigation of Fluorinated Amides for Solid-Electrolyte Interphase Stabilization in Li- O_2 Batteries Using Amide-Based Electrolytes. *J. Phys. Chem. C* **2013**, *117*, 11977–11988. [[CrossRef](#)]
29. Walker, W.; Giordani, V.; Uddin, J.; Bryantsev, V.S.; Chase, G.V.; Addison, D. A Rechargeable Li- O_2 Battery Using a Lithium Nitrate/*N,N*-Dimethylacetamide Electrolyte. *J. Am. Chem. Soc.* **2013**, *135*, 2076–2079. [[CrossRef](#)] [[PubMed](#)]
30. Roberts, M.; Younesi, R.; Richardson, W.; Liu, J.; Zhu, J.; Edstrom, K.; Gustafsson, T. Increased Cycling Efficiency of Lithium Anodes in Dimethyl Sulfoxide Electrolytes for Use in Li- O_2 Batteries. *ECS Electrochem. Lett.* **2014**, *3*, A62–A65. [[CrossRef](#)]
31. Zhang, T.; Liao, K.; He, P.; Zhou, H. A Self-Defense Redox Mediator for Efficient Lithium- O_2 Batteries. *Energy Environ. Sci.* **2016**, *9*, 1024–1030. [[CrossRef](#)]
32. Lim, H.; Song, H.; Kim, J.; Gwon, H.; Bae, Y.; Park, K.; Hong, J.; Kim, H.; Kim, T.; Kim, Y.H.; et al. Superior Rechargeability and Efficiency of Lithium–Oxygen Batteries: Hierarchical Air Electrode Architecture Combined with a Soluble Catalyst. *Angew. Chem.-Int. Ed.* **2014**, *53*, 3926–3931. [[CrossRef](#)] [[PubMed](#)]
33. Huang, Z.; Ren, J.; Zhang, W.; Xie, M.; Li, Y.; Sun, D.; Shen, Y.; Huang, Y. Protecting the Li-Metal Anode in a Li- O_2 Battery by Using Boric Acid as an SEI-Forming Additive. *Adv. Mater.* **2018**, *30*, 1803270. [[CrossRef](#)] [[PubMed](#)]
34. Zhang, Y.; Wang, L.; Guo, Z.; Xu, Y.; Wang, Y.; Peng, H. High-Performance Lithium-Air Battery with a Coaxial-Fiber Architecture. *Angew. Chem.-Int. Ed.* **2016**, *55*, 4487–4491. [[CrossRef](#)] [[PubMed](#)]
35. Huang, Y.; Geng, J.; Jiang, Z.; Ren, M.; Wen, B.; Chen, J.; Li, F. Solvation Structure with Enhanced Anionic Coordination for Stable Anodes in Lithium-Oxygen Batteries. *Angew. Chem. Int. Ed.* **2023**, *62*, e202306236. [[CrossRef](#)] [[PubMed](#)]
36. Kichambare, P.; Rodrigues, S.; Kumar, J. Mesoporous Nitrogen-Doped Carbon-Glass Ceramic Cathodes for Solid-State Lithium–Oxygen Batteries. *ACS Appl. Mater. Interfaces* **2012**, *4*, 49–52. [[CrossRef](#)]

37. Kitaura, H.; Zhou, H. Electrochemical Performance and Reaction Mechanism of All-Solid-State Lithium-Air Batteries Composed of Lithium, $\text{Li}_{1+x}\text{Al}_y\text{Ge}_{2-y}(\text{PO}_4)_3$ Solid Electrolyte and Carbon Nanotube Air Electrode. *Energy Environ. Sci.* **2012**, *5*, 9077. [[CrossRef](#)]
38. Yi, J.; Liu, X.; Guo, S.; Zhu, K.; Xue, H.; Zhou, H. Novel Stable Gel Polymer Electrolyte: Toward a High Safety and Long Life Li-Air Battery. *ACS Appl. Mater. Interfaces* **2015**, *7*, 23798–23804. [[CrossRef](#)] [[PubMed](#)]
39. Jang, I.C.; Ida, S.; Ishihara, T. Surface Coating Layer on Li Metal for Increased Cycle Stability of Li-O₂ Batteries. *J. Electrochem. Soc.* **2014**, *161*, A821–A826. [[CrossRef](#)]
40. Wu, J.; Li, M.; Gao, S.; Dou, Y.; Pan, K.; Zhang, Z.; Zhou, Z. Electrospinning-Assisted Porous Skeleton Electrolytes for Semi-Solid Li-O₂ Batteries. *Chem. Commun.* **2024**, *60*, 5070–5073. [[CrossRef](#)]
41. Amici, J.; Alidoost, M.; Caldera, F.; Versaci, D.; Zubair, U.; Trotta, F.; Francia, C.; Bodoardo, S. PEEK-WC/Nanosponge Membranes for Lithium-Anode Protection in Rechargeable Li-O₂ Batteries. *ChemElectroChem* **2018**, *5*, 1599–1605. [[CrossRef](#)]
42. Park, S.H.; Lee, T.H.; Lee, Y.J.; Park, H.B.; Lee, Y.J. Graphene Oxide Sieving Membrane for Improved Cycle Life in High-Efficiency Redox-Mediated Li-O₂ Batteries. *Small* **2018**, *14*, 1801456. [[CrossRef](#)] [[PubMed](#)]
43. Kim, Y.; Koo, D.; Ha, S.; Jung, S.C.; Yim, T.; Kim, H.; Oh, S.K.; Kim, D.-M.; Choi, A.; Kang, Y.; et al. Two-Dimensional Phosphorene-Derived Protective Layers on a Lithium Metal Anode for Lithium-Oxygen Batteries. *ACS Nano* **2018**, *12*, 4419–4430. [[CrossRef](#)] [[PubMed](#)]
44. Asadi, M.; Sayahpour, B.; Abbasi, P.; Ngo, A.T.; Karis, K.; Jokisaari, J.R.; Liu, C.; Narayanan, B.; Gerard, M.; Yasaei, P.; et al. A Lithium-Oxygen Battery with a Long Cycle Life in an Air-like Atmosphere. *Nature* **2018**, *555*, 502–506. [[CrossRef](#)] [[PubMed](#)]
45. Lim, H.-S.; Kwak, W.-J.; Chae, S.; Wi, S.; Li, L.; Hu, J.; Tao, J.; Wang, C.; Xu, W.; Zhang, J.-G. Stable Solid Electrolyte Interphase Layer Formed by Electrochemical Pretreatment of Gel Polymer Coating on Li Metal Anode for Lithium-Oxygen Batteries. *ACS Energy Lett.* **2021**, *6*, 3321–3331. [[CrossRef](#)]
46. Shi, L.; Li, Z.; Li, Y.; Wang, G.; Wu, M.; Wen, Z. Suppressing Redox Shuttle with MXene-Modified Separators for Li-O₂ Batteries. *ACS Appl. Mater. Interfaces* **2021**, *13*, 30766–30775. [[CrossRef](#)] [[PubMed](#)]
47. Zhu, J.; Yang, J.; Zhou, J.; Zhang, T.; Li, L.; Wang, J.; Nuli, Y. A Stable Organic-Inorganic Hybrid Layer Protected Lithium Metal Anode for Long-Cycle Lithium-Oxygen Batteries. *J. Power Sources* **2017**, *366*, 265–269. [[CrossRef](#)]
48. Wang, J.; Yang, M.; Zou, G.; Liu, D.; Peng, Q. Lithiation MXene Derivative Skeletons for Wide-Temperature Lithium Metal Anodes. *Adv. Funct. Mater.* **2021**, *31*, 2101180. [[CrossRef](#)]
49. Wang, J.; Yang, M.; Wang, J.; Liu, D.; Zou, G.; Liu, B.; Tse, J.S.; Li, L.; Ren, L.; Peng, Q. Lithiation MAX Derivative Electrodes with Low Overpotential and Long-Term Cyclability in a Wide-Temperature Range. *Energy Storage Mater.* **2022**, *47*, 611–619. [[CrossRef](#)]
50. Liu, J.; Bai, L.; He, J.; Wang, C.; Li, Q.; Song, F.; Hong, Z.; Chen, Y.; Zeng, F.; Cheng, C.; et al. Interfacial Polymerization-Modified Polyetherimide (PEI) Separator for Li-O₂ Battery with Boosted Performance. *ACS Appl. Polym. Mater.* **2022**, *4*, 5781–5788. [[CrossRef](#)]
51. Sun, Y.; Chen, K.; Zhang, C.; Yu, H.; Wang, X.; Yang, D.; Wang, J.; Huang, G.; Zhang, S. A Novel Material for High-Performance Li-O₂ Battery Separator: Polyetherketone Nanofiber Membrane. *Small* **2022**, *18*, 2201470. [[CrossRef](#)] [[PubMed](#)]
52. Abraham, K.M.; Jiang, Z. A Polymer Electrolyte-Based Rechargeable Lithium/Oxygen Battery. *J. Electrochem. Soc.* **1996**, *143*, 1–5. [[CrossRef](#)]
53. Luo, L.; Liu, B.; Song, S.; Xu, W.; Zhang, J.-G.; Wang, C. Revealing the Reaction Mechanisms of Li-O₂ Batteries Using Environmental Transmission Electron Microscopy. *Nat. Nanotechnol.* **2017**, *12*, 535–539. [[CrossRef](#)] [[PubMed](#)]
54. Peng, Z.; Freunberger, S.A.; Hardwick, L.J.; Chen, Y.; Giordani, V.; Bardé, F.; Novák, P.; Graham, D.; Tarascon, J.; Bruce, P.G. Oxygen Reactions in a Non-Aqueous Li⁺ Electrolyte. *Angew. Chem.-Int. Ed.* **2011**, *50*, 6351–6355. [[CrossRef](#)]
55. McCloskey, B.D.; Scheffler, R.; Speidel, A.; Bethune, D.S.; Shelby, R.M.; Luntz, A.C. On the Efficacy of Electrocatalysis in Nonaqueous Li-O₂ Batteries. *J. Am. Chem. Soc.* **2011**, *133*, 18038–18041. [[CrossRef](#)]
56. Zhang, S.S.; Foster, D.; Read, J. Discharge Characteristic of a Non-Aqueous Electrolyte Li/O₂ Battery. *J. Power Sources* **2010**, *195*, 1235–1240. [[CrossRef](#)]
57. Adams, B.D.; Radtke, C.; Black, R.; Trudeau, M.L.; Zaghib, K.; Nazar, L.F. Current Density Dependence of Peroxide Formation in the Li-O₂ Battery and Its Effect on Charge. *Energy Environ. Sci.* **2013**, *6*, 1772. [[CrossRef](#)]
58. McCloskey, B.D.; Speidel, A.; Scheffler, R.; Miller, D.C.; Viswanathan, V.; Hummelshej, J.S.; Nørskov, J.K.; Luntz, A.C. Twin Problems of Interfacial Carbonate Formation in Nonaqueous Li-O₂ Batteries. *J. Phys. Chem. Lett.* **2012**, *3*, 997–1001. [[CrossRef](#)] [[PubMed](#)]
59. Carboni, M.; Marrani, A.G.; Spezia, R.; Brutti, S. 1,2-Dimethoxyethane Degradation Thermodynamics in Li-O₂ Redox Environments. *Chem.-Eur. J.* **2016**, *22*, 17188–17203. [[CrossRef](#)] [[PubMed](#)]
60. Mahne, N.; Schafzahl, B.; Leybold, C.; Leybold, M.; Grumm, S.; Leitgeb, A.; Strohmeier, G.A.; Wilkening, M.; Fontaine, O.; Kramer, D.; et al. Singlet Oxygen Generation as a Major Cause for Parasitic Reactions during Cycling of Aprotic Lithium-Oxygen Batteries. *Nat. Energy* **2017**, *2*, 17036. [[CrossRef](#)]
61. Kim, J.-H.; Kannan, A.G.; Woo, H.-S.; Jin, D.-G.; Kim, W.; Ryu, K.; Kim, D.-W. A Bi-Functional Metal-Free Catalyst Composed of Dual-Doped Graphene and Mesoporous Carbon for Rechargeable Lithium-Oxygen Batteries. *J. Mater. Chem. A* **2015**, *3*, 18456–18465. [[CrossRef](#)]
62. Lou, P.; Cui, Z.; Guo, X. Achieving Highly Stable Li-O₂ Battery Operation by Designing a Carbon Nitride-Based Cathode towards a Stable Reaction Interface. *J. Mater. Chem. A* **2017**, *5*, 18207–18213. [[CrossRef](#)]

63. Zhan, Y.; Lu, M.; Yang, S.; Xu, C.; Liu, Z.; Lee, J.Y. Activity of Transition-Metal (Manganese, Iron, Cobalt, and Nickel) Phosphates for Oxygen Electrocatalysis in Alkaline Solution. *ChemCatChem* **2016**, *8*, 372–379. [[CrossRef](#)]
64. Ma, S.; Xie, M.; Lou, A.; Dong, Y.; Li, Z.; Lu, Y.; Liu, Q. Air Activation Enhances the Porosity and N,O Synergistic Effect towards an Efficient Metal Free Carbon Cathode for Li-O₂ Battery. *Electrochim. Acta* **2024**, *475*, 143660. [[CrossRef](#)]
65. Zhao, T.; Yao, Y.; Yuan, Y.; Wang, M.; Wu, F.; Amine, K.; Lu, J. A Universal Method to Fabricating Porous Carbon for Li-O₂ Battery. *Nano Energy* **2021**, *82*, 105782. [[CrossRef](#)]
66. Zhao, B.; Ye, Z.; Kong, X.; Han, L.; Xia, Z.; Chen, K.; Wang, Q.; Li, M.; Shang, Y.; Cao, A. Orthogonal-Channel, Low-Tortuosity Carbon Nanotube Platforms for High-Performance Li-O₂ Batteries. *ACS Nano* **2023**, *17*, 18382–18391. [[CrossRef](#)]
67. Shi, S.; Shen, Z.; Li, S.; Wang, Q.; Wen, R.; Liu, B. High-Yield Synthesis of Colloidal Carbon Rings and Their Applications in Self-Standing Electrodes of Li-O₂ Batteries. *J. Am. Chem. Soc.* **2023**, *145*, 27664–27671. [[CrossRef](#)] [[PubMed](#)]
68. Qin, L.; Lv, W.; Wei, W.; Kang, F.; Zhai, D.; Yang, Q.-H. Oxygen-Enriched Carbon Nanotubes as a Bifunctional Catalyst Promote the Oxygen Reduction/Evolution Reactions in Li-O₂ Batteries. *Carbon* **2019**, *141*, 561–567. [[CrossRef](#)]
69. Jo, H.-G.; Ahn, H.-J. Accelerating the Oxygen Reduction Reaction and Oxygen Evolution Reaction Activities of N and P Co-Doped Porous Activated Carbon for Li-O₂ Batteries. *Catalysts* **2020**, *10*, 1316. [[CrossRef](#)]
70. Jiang, Y.; Cheng, J.; Zou, L.; Li, X.; Gong, Y.; Chi, B.; Pu, J.; Li, J. In-Situ Growth of CeO₂ Nanoparticles on N-Doped Reduced Graphene Oxide for Anchoring Li₂O₂ Formation in Lithium-Oxygen Batteries. *Electrochim. Acta* **2016**, *210*, 712–719. [[CrossRef](#)]
71. Ma, S.; Wu, Y.; Wang, J.; Zhang, Y.; Zhang, Y.; Yan, X.; Wei, Y.; Liu, P.; Wang, J.; Jiang, K.; et al. Reversibility of Noble Metal-Catalyzed Aprotic Li-O₂ Batteries. *Nano Lett.* **2015**, *15*, 8084–8090. [[CrossRef](#)] [[PubMed](#)]
72. Ye, S.J.; Kim, D.Y.; Kim, D.W.; Park, O.O.; Kang, Y. Facile Synthesis of Palladium Nanodendrites Supported on Graphene Nanoplatelets: An Efficient Catalyst for Low Overpotentials in Lithium-Oxygen Batteries. *J. Mater. Chem. A* **2016**, *4*, 578–586. [[CrossRef](#)]
73. Xu, J.-J.; Wang, Z.-L.; Xu, D.; Zhang, L.-L.; Zhang, X.-B. Tailoring Deposition and Morphology of Discharge Products towards High-Rate and Long-Life Lithium-Oxygen Batteries. *Nat. Commun.* **2013**, *4*, 2438. [[CrossRef](#)] [[PubMed](#)]
74. Jian, Z.; Liu, P.; Li, F.; He, P.; Guo, X.; Chen, M.; Zhou, H. Core-Shell-Structured CNT@RuO₂ Composite as a High-Performance Cathode Catalyst for Rechargeable Li-O₂ Batteries. *Angew. Chem.-Int. Ed.* **2014**, *53*, 442–446. [[CrossRef](#)] [[PubMed](#)]
75. Liao, K.; Wang, X.; Sun, Y.; Tang, D.; Han, M.; He, P.; Jiang, X.; Zhang, T.; Zhou, H. An Oxygen Cathode with Stable Full Discharge-Charge Capability Based on 2D Conducting Oxide. *Energy Environ. Sci.* **2015**, *8*, 1992–1997. [[CrossRef](#)]
76. Zhou, Y.; Yin, K.; Gu, Q.; Tao, L.; Li, Y.; Tan, H.; Zhou, J.; Zhang, W.; Li, H.; Guo, S. Lewis-Acidic PtIr Multipods Enable High-Performance Li-O₂ Batteries. *Angew. Chem.-Int. Ed.* **2021**, *60*, 26592–26598. [[CrossRef](#)] [[PubMed](#)]
77. Lu, J.; Jung Lee, Y.; Luo, X.; Chun Lau, K.; Asadi, M.; Wang, H.-H.; Brombosz, S.; Wen, J.; Zhai, D.; Chen, Z.; et al. A Lithium-Oxygen Battery Based on Lithium Superoxide. *Nature* **2016**, *529*, 377–382. [[CrossRef](#)] [[PubMed](#)]
78. Qiao, Y.; Yi, J.; Wu, S.; Liu, Y.; Yang, S.; He, P.; Zhou, H. Li-CO₂ Electrochemistry: A New Strategy for CO₂ Fixation and Energy Storage. *Joule* **2017**, *1*, 359–370. [[CrossRef](#)]
79. Liu, B.; Sun, Y.; Liu, L.; Chen, J.; Yang, B.; Xu, S.; Yan, X. Recent Advances in Understanding Li-CO₂ Electrochemistry. *Energy Environ. Sci.* **2019**, *12*, 887–922. [[CrossRef](#)]
80. Han, X.; Liu, Y.; Jia, Z.; Chen, Y.-C.; Wan, J.; Weadock, N.; Gaskell, K.J.; Li, T.; Hu, L. Atomic-Layer-Deposition Oxide Nanoglue for Sodium Ion Batteries. *Nano Lett.* **2014**, *14*, 139–147. [[CrossRef](#)] [[PubMed](#)]
81. Hu, X.; Luo, G.; Zhao, Q.; Wu, D.; Yang, T.; Wen, J.; Wang, R.; Xu, C.; Hu, N. Ru Single Atoms on N-Doped Carbon by Spatial Confinement and Ionic Substitution Strategies for High-Performance Li-O₂ Batteries. *J. Am. Chem. Soc.* **2020**, *142*, 16776–16786. [[CrossRef](#)] [[PubMed](#)]
82. Li, Y.; Li, Y.; Ding, Y.; Ma, J.; Das, P.; Zhang, B.; Wu, Z.-S.; Bao, X. Spatially Confined Sub-Nanometer Pt in RuO₂ Nanosheet as Robust Bifunctional Oxygen Electrocatalyst for Stabilizing Li-O₂ Batteries. *Chem Catal.* **2023**, *3*, 100658. [[CrossRef](#)]
83. Wang, Y.; Sun, Y.; Wu, F.; Zou, G.; Gaumet, J.-J.; Li, J.; Fernandez, C.; Wang, Y.; Peng, Q. Nitrogen-Anchored Boridene Enables Mg-CO₂ Batteries with High Reversibility. *J. Am. Chem. Soc.* **2024**, *146*, 9967–9974. [[CrossRef](#)] [[PubMed](#)]
84. Débart, A.; Bao, J.; Armstrong, G.; Bruce, P.G. An O₂ Cathode for Rechargeable Lithium Batteries: The Effect of a Catalyst. *J. Power Sources* **2007**, *174*, 1177–1182. [[CrossRef](#)]
85. Liu, Y.; Cai, J.; Zhou, J.; Zang, Y.; Zheng, X.; Zhu, Z.; Liu, B.; Wang, G.; Qian, Y. Tailoring the Adsorption Behavior of Superoxide Intermediates on Nickel Carbide Enables High-Rate Li-O₂ Batteries. *eScience* **2022**, *2*, 389–398. [[CrossRef](#)]
86. Zhou, Y.; Guo, S. Recent Advances in Cathode Catalyst Architecture for Lithium–Oxygen Batteries. *eScience* **2023**, *3*, 100123. [[CrossRef](#)]
87. Débart, A.; Paterson, A.J.; Bao, J.; Bruce, P.G. α -MnO₂ Nanowires: A Catalyst for the O₂ Electrode in Rechargeable Lithium Batteries. *Angew. Chem.-Int. Ed.* **2008**, *47*, 4521–4524. [[CrossRef](#)] [[PubMed](#)]
88. Guo, Z.; Zhu, G.; Qiu, Z.; Wang, Y.; Xia, Y. High Performance Li-O₂ Battery Using γ -MnOOH Nanorods as a Catalyst in an Ionic-Liquid Based Electrolyte. *Electrochim. Commun.* **2012**, *25*, 26–29. [[CrossRef](#)]
89. Zhang, G.Q.; Zheng, J.P.; Liang, R.; Zhang, C.; Wang, B.; Au, M.; Hendrickson, M.; Plichta, E.J. α -MnO₂/Carbon Nanotube/Carbon Nanofiber Composite Catalytic Air Electrodes for Rechargeable Lithium-Air Batteries. *J. Electrochem. Soc.* **2011**, *158*, A822. [[CrossRef](#)]

90. Jin, L.; Xu, L.; Morein, C.; Chen, C.; Lai, M.; Dharmarathna, S.; Dobley, A.; Suib, S.L. Titanium Containing γ -MnO₂ (TM) Hollow Spheres: One-Step Synthesis and Catalytic Activities in Li/Air Batteries and Oxidative Chemical Reactions. *Adv. Funct. Mater.* **2010**, *20*, 3373–3382. [CrossRef]
91. Cao, Y.; Wei, Z.; He, J.; Zang, J.; Zhang, Q.; Zheng, M.; Dong, Q. α -MnO₂ Nanorods Grown *in Situ* on Graphene as Catalysts for Li-O₂ Batteries with Excellent Electrochemical Performance. *Energy Environ. Sci.* **2012**, *5*, 9765. [CrossRef]
92. Morales-Guio, C.G.; Stern, L.-A.; Hu, X. Nanostructured Hydrotreating Catalysts for Electrochemical Hydrogen Evolution. *Chem. Soc. Rev.* **2014**, *43*, 6555. [CrossRef] [PubMed]
93. Xie, J.; Li, S.; Zhang, X.; Zhang, J.; Wang, R.; Zhang, H.; Pan, B.; Xie, Y. Atomically-Thin Molybdenum Nitride Nanosheets with Exposed Active Surface Sites for Efficient Hydrogen Evolution. *Chem. Sci.* **2014**, *5*, 4615–4620. [CrossRef]
94. Michalsky, R.; Zhang, Y.-J.; Peterson, A.A. Trends in the Hydrogen Evolution Activity of Metal Carbide Catalysts. *ACS Catal.* **2014**, *4*, 1274–1278. [CrossRef]
95. Ma, L.; Ting, L.R.L.; Molinari, V.; Giordano, C.; Yeo, B.S. Efficient Hydrogen Evolution Reaction Catalyzed by Molybdenum Carbide and Molybdenum Nitride Nanocatalysts Synthesized via the Urea Glass Route. *J. Mater. Chem. A* **2015**, *3*, 8361–8368. [CrossRef]
96. Zhao, Y.; Kamiya, K.; Hashimoto, K.; Nakanishi, S. In Situ CO₂-Emission Assisted Synthesis of Molybdenum Carbonitride Nanomaterial as Hydrogen Evolution Electrocatalyst. *J. Am. Chem. Soc.* **2015**, *137*, 110–113. [CrossRef] [PubMed]
97. Zhu, J.; Sakaushi, K.; Clavel, G.; Shalom, M.; Antonietti, M.; Fellinger, T.-P. A General Salt-Templating Method to Fabricate Vertically Aligned Graphitic Carbon Nanosheets and Their Metal Carbide Hybrids for Superior Lithium Ion Batteries and Water Splitting. *J. Am. Chem. Soc.* **2015**, *137*, 5480–5485. [CrossRef]
98. Wan, C.; Leonard, B.M. Iron-Doped Molybdenum Carbide Catalyst with High Activity and Stability for the Hydrogen Evolution Reaction. *Chem. Mater.* **2015**, *27*, 4281–4288. [CrossRef]
99. Wu, H.B.; Xia, B.Y.; Yu, L.; Yu, X.-Y.; Lou, X.W. Porous Molybdenum Carbide Nano-Octahedrons Synthesized via Confined Carburization in Metal-Organic Frameworks for Efficient Hydrogen Production. *Nat. Commun.* **2015**, *6*, 6512. [CrossRef] [PubMed]
100. Ma, F.; Wu, H.B.; Xia, B.Y.; Xu, C.; Lou, X.W. Hierarchical β -Mo₂C Nanotubes Organized by Ultrathin Nanosheets as a Highly Efficient Electrocatalyst for Hydrogen Production. *Angew. Chem. Int. Ed.* **2015**, *54*, 15395–15399. [CrossRef] [PubMed]
101. Xu, H.; Zheng, R.; Du, D.; Ren, L.; Wen, X.; Wang, X.; Tian, G.; Shu, C. Adjusting the 3d Orbital Occupation of Ti in Ti₃C₂ MXene via Nitrogen Doping to Boost Oxygen Electrode Reactions in Li-O₂ Battery. *Small* **2023**, *19*, 2206611. [CrossRef] [PubMed]
102. Yang, Y.; Yao, M.; Wang, X.; Huang, H. Theoretical Prediction of Catalytic Activity of Ti₂C MXene as Cathode for Li-O₂ Batteries. *J. Phys. Chem. C* **2019**, *123*, 17466–17471. [CrossRef]
103. Li, J.; Han, K.; Huang, J.; Li, G.; Peng, S.; Li, N.; Wang, J.; Zhang, W.; Du, Y.; Fan, Y.; et al. Polarized Nucleation and Efficient Decomposition of Li₂O₂ for Ti₂C MXene Cathode Catalyst under a Mixed Surface Condition in Lithium-Oxygen Batteries. *Energy Storage Mater.* **2021**, *35*, 669–678. [CrossRef]
104. Sun, Z.; Hu, Y.; Zhang, J.; Zhou, N.; Li, M.; Liu, H.; Huo, B.; Chao, M.; Zeng, K. Interfacial Oxygen Bridge Bonding with Mo-O-Ti Units in MoO_x@Ti₃C₂ MXene Harness Efficient Li-O₂ Battery at High Rate. *Appl. Catal. B Environ. Energy* **2024**, *351*, 123984. [CrossRef]
105. Li, J.; Zhou, H.; Jian, Z.; Li, H.; Guan, X.; Xing, Y.; Zhang, S.; Xu, H. Improved Electrocatalytic Activity of Three-Dimensional Open-Structured Co₃O₄@MnO₂ Bifunctional Catalysts of Li-O₂ Batteries by Inducing the Oriented Growth of Li₂O₂. *ACS Sustain. Chem. Eng.* **2021**, *9*, 5334–5344. [CrossRef]
106. Ma, Z.; Yuan, X.; Li, L.; Ma, Z.-F. The Double Perovskite Oxide Sr₂CrMoO₆– δ as an Efficient Electrocatalyst for Rechargeable Lithium Air Batteries. *Chem. Commun.* **2014**, *50*, 14855–14858. [CrossRef]
107. Yang, W.; Salim, J.; Li, S.; Sun, C.; Chen, L.; Goodenough, J.B.; Kim, Y. Perovskite Sr_{0.95}Ce_{0.05}CoO₃– δ Loaded with Copper Nanoparticles as a Bifunctional Catalyst for Lithium-Air Batteries. *J. Mater. Chem.* **2012**, *22*, 18902. [CrossRef]
108. Zhang, D.; Song, Y.; Du, Z.; Wang, L.; Li, Y.; Goodenough, J.B. Active LaNi_{1-x}Fe_xO₃ Bifunctional Catalysts for Air Cathodes in Alkaline Media. *J. Mater. Chem. A* **2015**, *3*, 9421–9426. [CrossRef]
109. Xu, J.-J.; Wang, Z.-L.; Xu, D.; Meng, F.-Z.; Zhang, X.-B. 3D Ordered Macroporous LaFeO₃ as Efficient Electrocatalyst for Li-O₂ Batteries with Enhanced Rate Capability and Cyclic Performance. *Energy Environ. Sci.* **2014**, *7*, 2213. [CrossRef]
110. Xu, J.; Xu, D.; Wang, Z.; Wang, H.; Zhang, L.; Zhang, X. Synthesis of Perovskite-Based Porous La_{0.75}Sr_{0.25}MnO₃ Nanotubes as a Highly Efficient Electrocatalyst for Rechargeable Lithium–Oxygen Batteries. *Angew. Chem.-Int. Ed.* **2013**, *52*, 3887–3890. [CrossRef] [PubMed]
111. Li, X.; Qian, Z.; Han, G.; Sun, B.; Zuo, P.; Du, C.; Ma, Y.; Huo, H.; Lou, S.; Yin, G. Perovskite LaCo_xMn_{1-x}O₃– σ with Tunable Defect and Surface Structures as Cathode Catalysts for Li-O₂ Batteries. *ACS Appl. Mater. Interfaces* **2020**, *12*, 10452–10460. [CrossRef] [PubMed]
112. Qiu, Q.; Pan, Z.-Z.; Yao, P.; Yuan, J.; Xia, C.; Zhao, Y.; Li, Y. A 98.2% Energy Efficiency Li-O₂ Battery Using a LaNi_{0.5}Co_{0.5}O₃ Perovskite Cathode with Extremely Fast Oxygen Reduction and Evolution Kinetics. *Chem. Eng. J.* **2023**, *452*, 139608. [CrossRef]
113. Tao, L.; Sun, M.; Zhou, Y.; Luo, M.; Lv, F.; Li, M.; Zhang, Q.; Gu, L.; Huang, B.; Guo, S. A General Synthetic Method for High-Entropy Alloy Subnanometer Ribbons. *J. Am. Chem. Soc.* **2022**, *144*, 10582–10590. [CrossRef] [PubMed]
114. Zhang, P.; Hui, X.; Nie, Y.; Wang, R.; Wang, C.; Zhang, Z.; Yin, L. New Conceptual Catalyst on Spatial High-Entropy Alloy Heterostructures for High-Performance Li-O₂ Batteries. *Small* **2023**, *19*, 2206742. [CrossRef] [PubMed]

115. Tian, J.; Rao, Y.; Shi, W.; Yang, J.; Ning, W.; Li, H.; Yao, Y.; Zhou, H.; Guo, S. Sabatier Relations in Electrocatalysts Based on High-Entropy Alloys with Wide-Distributed d-Band Centers for Li-O₂ Batteries. *Angew. Chem.-Int. Ed.* **2023**, *62*, e202310894. [[CrossRef](#)] [[PubMed](#)]
116. Zhou, Y.; Gu, Q.; Xin, Y.; Tang, X.; Wu, H.; Guo, S. Orbital Coupling of PbO₇ Node in Single-Crystal Metal–Organic Framework Enhances Li-O₂ Battery Electrocatalysis. *Nano Lett.* **2023**, *23*, 10600–10607. [[CrossRef](#)] [[PubMed](#)]
117. Xing, S.; Zhang, Z.; Dou, Y.; Li, M.; Wu, J.; Zhang, Z.; Zhou, Z. An Efficient Multifunctional Soluble Catalyst for Li-O₂ Batteries. *CCS Chem.* **2024**, *6*, 1810–1820. [[CrossRef](#)]

Disclaimer/Publisher’s Note: The statements, opinions and data contained in all publications are solely those of the individual author(s) and contributor(s) and not of MDPI and/or the editor(s). MDPI and/or the editor(s) disclaim responsibility for any injury to people or property resulting from any ideas, methods, instructions or products referred to in the content.